Cooperative coupling of static magnetism and bulk superconductivity in the stripe phase of $La_{2-x}Ba_xCuO_4$: Pressure- and doping-dependent studies

Z. Guguchia,[1,2,*] R. Khasanov,[1] A. Shengelaya,[3,4] E. Pomjakushina,[5] S. J. L. Billinge,[6] A. Amato,[1] E. Morenzoni,[1] and H. Keller[7]

[1]*Laboratory for Muon Spin Spectroscopy, Paul Scherrer Institute, CH-5232 Villigen PSI, Switzerland*
[2]*Department of Physics, Columbia University, New York, New York 10027, USA*
[3]*Department of Physics, Tbilisi State University, Chavchavadze 3, GE-0128 Tbilisi, Georgia*
[4]*Andronikashvili Institute of Physics of I.Javakhishvili Tbilisi State University, Tamarashvili str. 6, 0177 Tbilisi, Georgia*
[5]*Laboratory for Developments and Methods, Paul Scherrer Institut, CH-5232 Villigen PSI, Switzerland*
[6]*Condensed Matter Physics and Materials Science Department, Brookhaven National Laboratory, Upton, New York 11973, USA*
[7]*Physik-Institut der Universität Zürich, Winterthurerstrasse 190, CH-8057 Zürich, Switzerland*

(Received 21 March 2016; revised manuscript received 19 October 2016; published 20 December 2016)

Static spin-stripe order and superconductivity were systematically studied in $La_{2-x}Ba_xCuO_4$ ($0.11 \leqslant x \leqslant 0.17$) at ambient pressure by means of magnetization and μSR experiments. We find that all the investigated $La_{2-x}Ba_xCuO_4$ samples exhibit static spin-stripe order and that the quasi-two-dimensional superconducting (SC) transition temperature T_{c1} and the static spin-stripe order temperature T_{so} have very similar values throughout the phase diagram. Moreover, the magnetic and the SC properties of the $x = 0.155$ (LBCO-0.155) and $x = 0.17$ (LBCO-0.17) samples were studied under hydrostatic pressure. As a remarkable result, in these bulk cuprate superconductors, the three-dimensional SC transition temperature T_c and T_{so} nearly coincide [$T_c(p) \simeq T_{so}(p)$] at all pressure investigated ($0 \leqslant p \leqslant 2.3$ GPa). We also observed a pressure induced transition from long-range spin stripe order to a disordered magnetic state at $p^\star \simeq 1.6$ GPa in LBCO-0.155, coexisting with a SC state with substantial superfluid density. In LBCO-0.17, a disordered magnetic state is present at all p. The present results indicate that static magnetic order and SC pairing correlations develop in a cooperative fashion in $La_{2-x}Ba_xCuO_4$, and provide a new route of understanding the complex interplay between static magnetism and superconductivity in the stripe phase of cuprates.

DOI: 10.1103/PhysRevB.94.214511

I. INTRODUCTION

Cuprate high-temperature superconductors (HTSs) have complex phase diagrams with multiple competing ordered phases. One of the most astonishing manifestations of this competition occurs in the system $La_{2-x}Ba_xCuO_4$ (LBCO) [1], where the bulk superconducting (SC) transition temperature T_c exhibits a deep minimum at $x = 1/8$ [2–4]. At this doping level, neutron and x-ray diffraction experiments revealed two-dimensional static charge and spin-stripe order [5–10]. While the relevance of stripe correlations for high-temperature superconductivity remains a subject of controversy, the collected experimental data indicate that the tendency toward unidirectional stripelike ordering is common to cuprates [3,4,11,12]. Exploring the role of stripe formation for the occurrence of high-temperature superconductivity in cuprates is paramount to elucidate the microscopic pairing mechanism.

On the experimental front, quasi-two-dimensional superconducting correlations were observed in $La_{1.875}Ba_{0.125}CuO_4$ (LBCO-1/8) and $La_{1.48}Nd_{0.4}Sr_{0.12}CuO_4$, coexisting with the ordering of static spin stripes, but with frustrated phase order between the layers [13–17]. On the theoretical front, the concept of a sinusoidally modulated [pair-density wave (PDW)] SC order (with the same period as the spin correlations so that its amplitude varies from positive to negative) was introduced, which is intimately intertwined with spatially modulated antiferromagnetism [18–20]. It has been proposed that both the PDW and the uniform d-wave states are close competitors for the SC ground state [18–20].

Motivated by the question whether the PDW state is relevant at hole concentrations $x \neq 1/8$ in $La_{2-x}Ba_xCuO_4$, Xu *et al.* investigated the system $La_{2-x}Ba_xCuO_4$ with $x = 0.095$ using inelastic neutron scattering [21]. In this bulk superconductor with $T_c = 32$ K low energy, incommensurate quasistatic antiferromagnetic spin correlations were observed. The coexistence of bulk superconductivity and antiferromagnetic (AFM) spin correlations was explained in terms of a spatially modulated and intertwined pair wave function [18–21]. There are only a few reports proposing the relevance of a PDW state in sufficiently underdoped $La_{2-x}Sr_xCuO_4$ [22] and $YBa_2Cu_3O_{6-x}$ [23,24]. At present, it is still unclear to what extent PDW order is a common feature of cuprate systems where stripe order occurs.

Recently, magnetism and superconductivity in LBCO-1/8, where the stripe order is most stable and magnetism occupies nearly the full volume of the sample, were studied by means of the muon-spin rotation (μSR) technique as a function of pressure up to $p \simeq 2.2$ GPa [25]. It was found that application of hydrostatic pressure leads to a remarkable decrease/increase of the magnetic/SC volume fraction. However, even at the highest applied pressure, the spin order is long range and occupies a substantial fraction of the sample. Because of the pressure limit, we were not able to investigate whether it is possible to completely suppress magnetic order and fully restore superconductivity in the stripe phase under pressure. Such an investigation will give important hints for the relevance of the concept of intertwined coexistence of magnetism and superconductivity in striped cuprates.

*zurab.guguchia@psi.ch

In this work, static spin-stripe order and superconductivity were systematically studied in polycrystalline samples of $La_{2-x}Ba_xCuO_4$ ($0.11 \leqslant x \leqslant 0.17$) at ambient pressure by means of magnetization and μSR experiments. We find that for all the investigated $La_{2-x}Ba_xCuO_4$ specimens a substantial fraction of the sample is magnetic and that the 2D SC transition temperature T_{c1} and the static spin-stripe order temperature T_{so} have very similar values throughout the phase diagram. An antagonistic doping dependence of the magnetic volume fraction V_m and the diamagnetic susceptibility χ_{ZFC} was also observed. Furthermore, we report on high pressure μSR ($p_{max} = 2.2$ GPa) and magnetization ($p_{max} = 3.1$ GPa) studies of the magnetic and superconducting properties of $x = 0.155$ (LBCO-0.155) and $x = 0.17$ (LBCO-0.17) samples. We choose these particular compositions ($x > 1/8$) for the high-pressure experiments, since they are good superconductors with a well defined single SC transitions and at the same time exhibit magnetic order. LBCO-0.155 also exhibits charge order as previously shown by x-ray and neutron diffraction experiments [8].

Remarkably, both T_c and T_{so} exhibit a similar pressure dependence in both systems, i.e., $T_c(p) \simeq T_{so}(p)$, which is an interesting finding. Antagonistic pressure dependence of the magnetic volume fraction V_m and the superfluid density ρ_s as well as the diamagnetic moment is also observed, similar to the case of x doping. This suggests phase separation between the SC and the magnetic ground state in $La_{2-x}Ba_xCuO_4$. The observed phase separation and the simultaneous appearance of static magnetism and superconductivity in $La_{2-x}Ba_xCuO_4$ ($0.11 \leqslant x \leqslant 0.17$) at ambient pressure and in $x = 0.155$ and 0.17 under hydrostatic pressures indicate that static order and SC pairing correlations develop in a cooperative fashion in $La_{2-x}Ba_xCuO_4$, forming a spatially self-organized pattern.

II. EXPERIMENTAL DETAILS

A. Sample preparation

Polycrystalline samples of $La_{2-x}Ba_xCuO_4$ with $x = 0.11$, 0.115, 0.125, 0.135, 0.145, 0.15, 0.155, and 0.17 were prepared by the conventional solid-state reaction method using La_2O_3, $BaCO_3$, and CuO. The single-phase character of the samples was checked by powder x-ray diffraction. All the measurements were performed on samples from the same batch.

B. Instruments

μSR experiments under pressure were performed at the GPD instrument (μE1 beamline) of the Paul Scherrer Institute (Villigen, Switzerland) [26]. The low-background GPS (πM3 beamline) and Dolly (πE1 beamline) instruments were used to study the systems $La_{2-x}Ba_xCuO_4$ at ambient pressure.

C. Pressure cells for μSR and magnetization experiments

The magnetic susceptibility for LBCO-0.155 was measured under pressures up to 3.1 GPa by a SQUID magnetometer (Quantum Design MPMS-XL). Pressures were generated using a diamond anvil cell (DAC) [27] filled with Daphne oil, which served as a pressure-transmitting medium. The pressure at low temperatures was determined by detecting the pressure dependence of the SC transition temperature of Pb. The magnetic susceptibilities for the rest of the samples $La_{2-x}Ba_xCuO_4$ were measured only at ambient pressure.

Pressures up to 2.3 GPa were generated in a double wall piston-cylinder type of cell made of MP35N material, especially designed to perform μSR experiments under pressure [26,28,29]. Cells with 6 mm ($p_{max} \simeq 2.3$ GPa) and 7 mm ($p_{max} \simeq 1.9$ GPa) of inner diameters were used for the LBCO-0.155 and LBCO-0.17 samples, respectively. As a pressure transmitting medium Daphne oil was used. The pressure was measured by tracking the SC transition of a very small indium plate by AC susceptibility. The filling factor of the pressure cell was maximized. The fraction of the muons stopping in the sample was approximately 40% and 50% for LBCO-0.155 and LBCO-0.17, respectively.

D. Analysis of zero-field (ZF) μSR data

In the pressure experiment a substantial fraction of the μSR asymmetry originates from muons stopping in the MP35N pressure cell surrounding the sample. Therefore the μSR data in the whole temperature range were analyzed by decomposing the signal into a contribution of the sample and a contribution of the pressure cell:

$$A(t) = A_S(0)P_S(t) + A_{PC}(0)P_{PC}(t), \tag{1}$$

where $A_S(0)$ and $A_{PC}(0)$ are the initial asymmetries and $P_S(t)$ and $P_{PC}(t)$ are the muon-spin polarizations belonging to the sample and the pressure cell, respectively. The pressure cell signal was analyzed by a damped Kubo-Toyabe function [28]. The response of the sample consists of a magnetic and a nonmagnetic contribution:

$$P_S(t) = V_m\left[\tfrac{2}{3}e^{-\lambda_T t}J_0(\gamma_\mu B_\mu t) + \tfrac{1}{3}e^{-\lambda_L t}\right] + (1 - V_m)e^{-\lambda_{nm} t}. \tag{2}$$

Here, V_m denotes the relative volume of the magnetic fraction and B_μ is the average internal magnetic field at the muon site. λ_T and λ_L are the depolarization rates representing the transversal and the longitudinal relaxing components of the magnetic parts of the sample. J_0 is the zeroth-order Bessel function of the first kind. This is characteristic for an incommensurate spin density wave and has been observed in cuprates with static spin stripe order [30]. λ_{nm} is the relaxation rate of the nonmagnetic part of the sample. The total initial asymmetry $A_{tot} = A_S(0) + A_{PC}(0) \simeq 0.285$ is a temperature independent constant. A typical fraction of muons stopped in the sample was $A_S(0)/A_{tot} \simeq 0.40(3)$ and $A_S(0)/A_{tot} \simeq 0.50(3)$, for $x = 0.155$ and 0.17, respectively, which was assumed to be temperature independent in the analysis. The μSR time spectra were analyzed using the free software package MUSRFIT [31].

E. Analysis of weak transverse field (WTF) μSR data

The TF-μSR spectra were fitted in the time domain with a combination of a slowly relaxing signal with a precession frequency corresponding to the applied field of $\mu_0 H = 3$ mT (due to muons in a paramagnetic environment) and a fast

relaxing signal due to muons precessing in much larger static local fields:

$$A_0 P(t) = (A_{PC} e^{-\lambda_{PC} t} + A_S^{'} e^{-\lambda^{'} t}) \cos(\gamma_\mu B^{'} t) + A_S^{''} \left[\tfrac{2}{3} e^{-\lambda_T^{''} t} J_0(\gamma_\mu B^{''} t) + \tfrac{1}{3} e^{-\lambda_L^{''} t} \right], \quad (3)$$

where A_0 is the initial asymmetry, $P(t)$ is the muon spin-polarization function, and $\gamma_\mu/(2\pi) \simeq 135.5$ MHz/T is the muon gyromagnetic ratio. A_{PC} and λ_{PC} are the asymmetry and the relaxation rate of the pressure cell signal. $A_S^{'}$ and $A_S^{''}$ are the asymmetries of the slowly and fast relaxing sample signals, respectively. $\lambda^{'}$ is the relaxation rate of the paramagnetic part of the sample. $\lambda_T^{''}$ and $\lambda_L^{''}$ are the transverse and the longitudinal relaxation rates, respectively, of the magnetic part of the sample. $B^{'}$ and $B^{''}$ are the magnetic fields, probed by the muons stopped in the paramagnetic and magnetic parts of the sample, respectively.

III. RESULTS

A. Superconductivity and static spin-stripe order in $La_{2-x}Ba_xCuO_4$ ($0.11 \leqslant x \leqslant 0.17$)

Figure 1 shows the temperature dependence of the zero-field-cooled (ZFC) magnetic susceptibility χ_{ZFC} for $La_{2-x}Ba_xCuO_4$ ($0.11 \leqslant x \leqslant 0.17$) samples recorded in a magnetic field of $\mu_0 H = 0.5$ mT. For the samples with $x = 0.11, 0.115, 0.125, 0.135, 0.145$, and 0.15 the diamagnetic moment exhibits a two-step SC transition, as observed in our previous works for $x = 0.125$ [25,32]. For $x = 0.125$, the first transition appears at $T_{c1} \simeq 30$ K and the second transition at $T_{c2} \simeq 5$ K with a larger diamagnetic response. Detailed investigations performed on single crystalline samples of LBCO-1/8 provided an explanation for this two-step SC transition [14]. The authors interpreted the transition at T_{c1} as due to the development of 2D superconductivity in the CuO_2 planes, while the interlayer Josephson coupling is frustrated by static stripes. A transition to a 3D SC phase takes place at a much lower temperature $T_{c2} \ll T_{c1}$. The values of T_{c1} and T_{c2} were defined as the temperatures where the linearly extrapolated magnetic moments intersect the zero line (see Fig. 1). Note that for the samples with $x = 0.155$ and 0.17, we observed a well defined single SC transition.

Figure 2(a) shows representative zero-field (ZF) μSR time spectra for polycrystalline $La_{2-x}Ba_xCuO_4$ ($0.11 \leqslant x \leqslant 0.17$) samples, recorded at 5 K. The μSR time spectra for all x are well described by a zeroth-order Bessel function, which is characteristic for an incommensurate spin density wave, suggesting the presence of static spin-stripe order in $La_{2-x}Ba_xCuO_4$ ($0.11 \leqslant x \leqslant 0.17$). In a long-range ordered magnetic system, a coherent muon precession of the whole ensemble is observed giving rise to oscillations in the ZF μSR time spectra as it is the case for all the investigated $La_{2-x}Ba_xCuO_4$ samples, except the one with $x = 0.17$. A damping of the μSR oscillation indicates a distribution of internal magnetic fields sensed by the muon ensemble and is therefore a measure of the disorder in the magnetic system. It is evident that the μSR precession is strongly damped and no coherent precession signal is observed for LBCO-0.17, indicating the presence of a disordered magnetic state in this system. Figure 2(b) shows the ZF μSR time spectra for the $x = 0.15$ sample, which demonstrates the appearance of the magnetic order below ~30 K. Figure 3(a) shows the temperature dependence of the magnetic volume fraction V_m extracted from the ZF-μSR data for polycrystalline $La_{2-x}Ba_xCuO_4$ ($0.11 \leqslant x \leqslant 0.17$). These data reveal that for all the investigated $La_{2-x}Ba_xCuO_4$ specimens a substantial

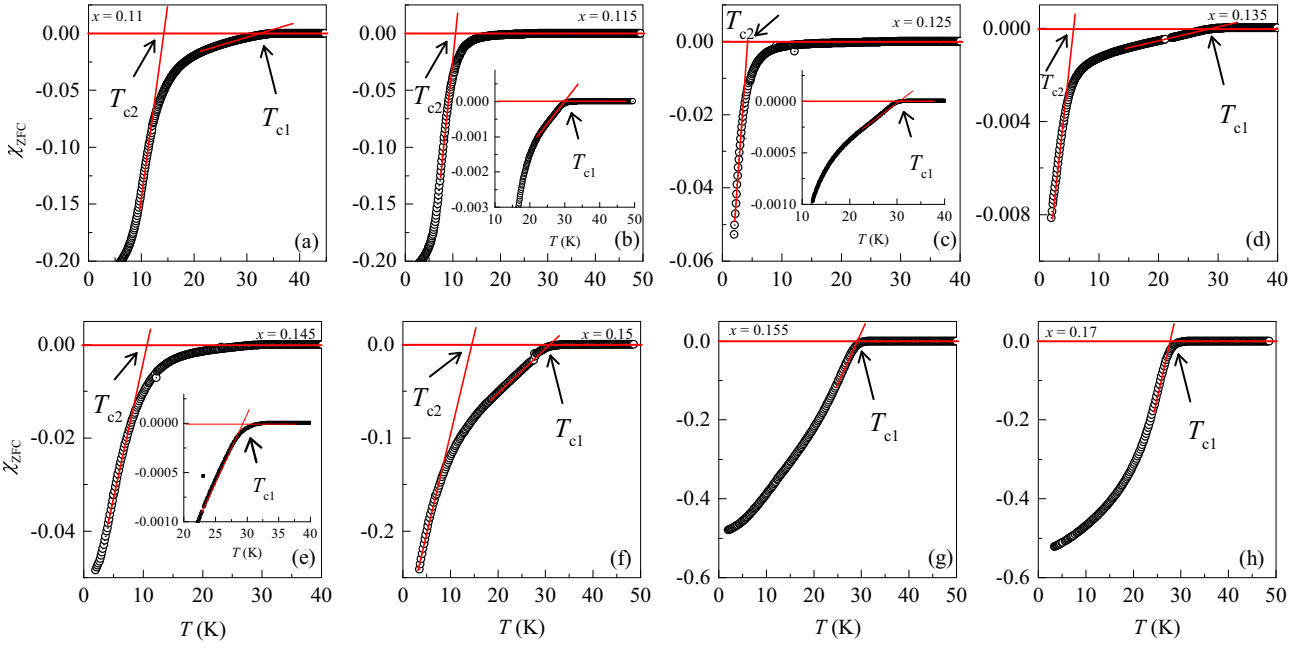

FIG. 1. Temperature dependence of the diamagnetic susceptibility χ_{ZFC} of $La_{2-x}Ba_xCuO_4$ for various x, measured at ambient pressures in a magnetic field of $\mu_0 H = 0.5$ mT. The arrows denote the superconducting transition temperatures T_{c1} and T_{c2}. The insets show the SC transition near T_{c1}.

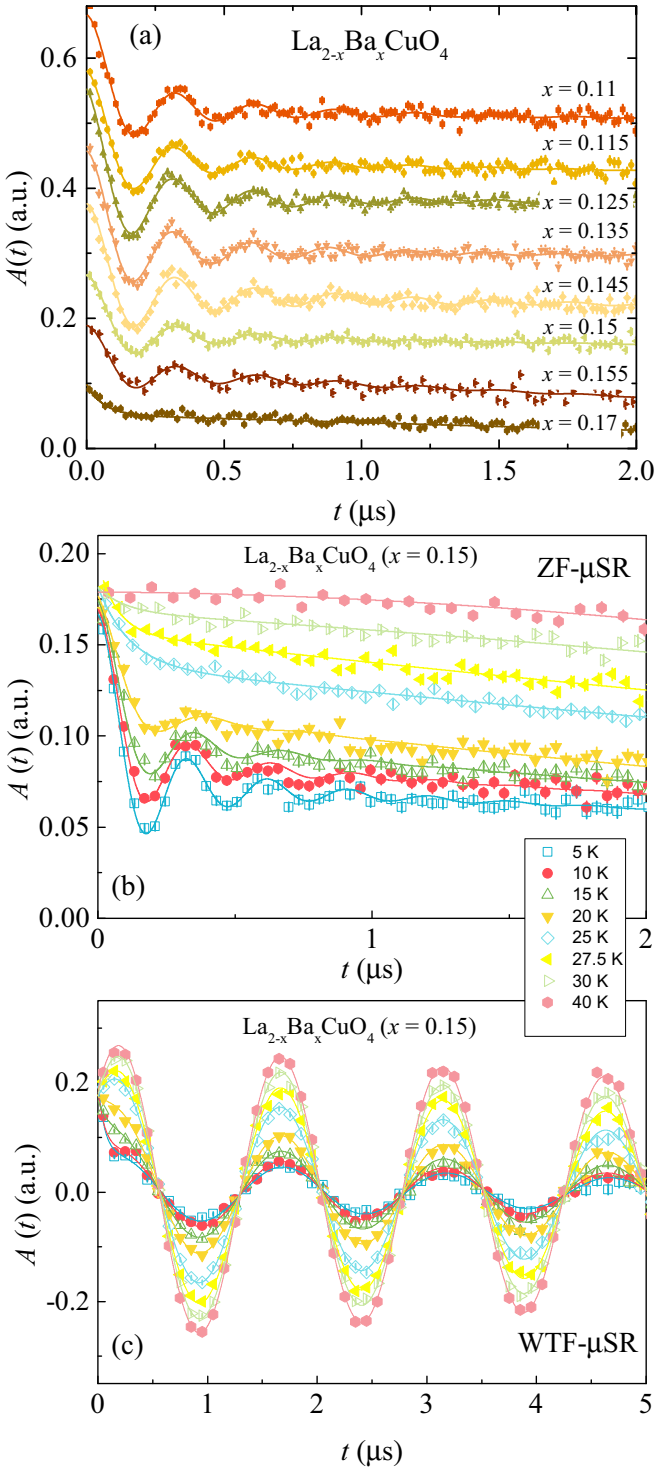

FIG. 2. (a) ZF μSR time spectra $A(t)$ for $La_{2-x}Ba_xCuO_4$ at various x, recorded at 5 K. ZF μSR (b) and WTF μSR (c) spectra for the $x = 0.15$ sample, recorded at various temperatures.

fraction of the sample is magnetic with a relatively high spin-order temperature.

Transverse-field (TF) μSR experiments in weak transverse field (WTF-μSR) were also carried out in order to extract T_{so} and compare the values to the ones extracted from the ZF-μSR. Figure 2(c) shows the WTF μSR time spectra for the $x = 0.15$ sample, which clearly shows the reduction of the amplitude of

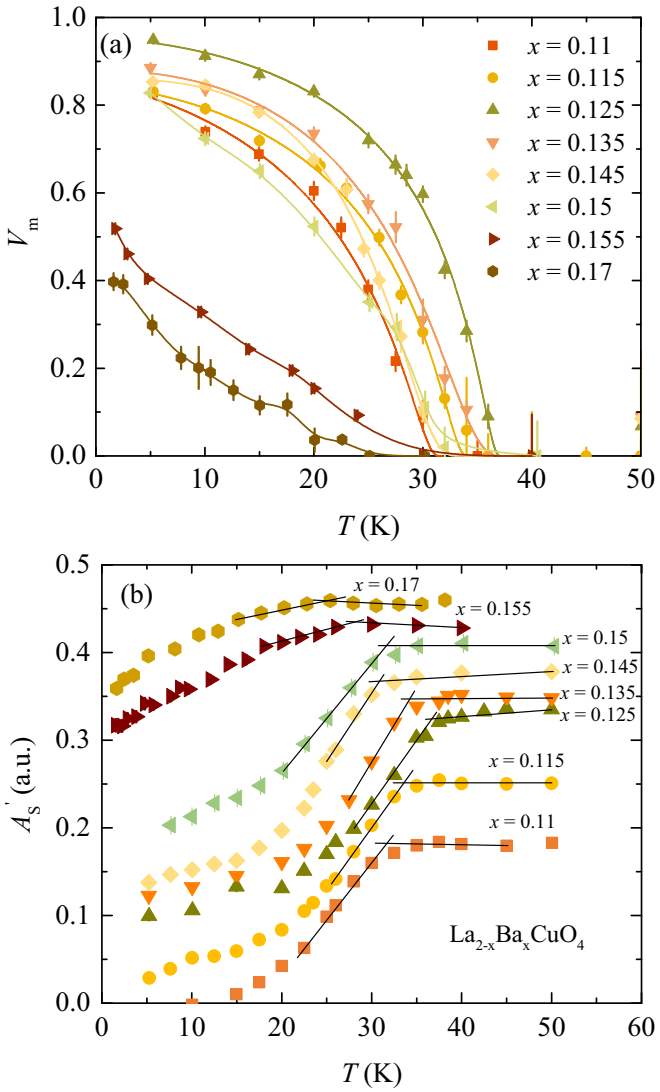

FIG. 3. (a) Temperature dependence of the magnetic volume fraction V_m in $La_{2-x}Ba_xCuO_4$ for various x, determined from ZF μSR. (b) The WTF μSR asymmetry for $La_{2-x}Ba_xCuO_4$ ($0.11 \leqslant x \leqslant 0.17$) is plotted as a function of temperature in an applied field of $\mu_0 H = 3$ mT. The onset temperature to the magnetically ordered state T_{so} is defined as the temperatures where the linearly extrapolated low- and high-temperature data points intersect (indicated by the straight lines).

the μSR signal upon lowering the temperature below ~30 K, indicating the appearance of the magnetic order. Figure 3(b) shows the WTF-μSR asymmetry for $La_{2-x}Ba_xCuO_4$ ($0.11 \leqslant x \leqslant 0.17$), extracted from the WTF μSR spectra, (following the procedure given in Sec. III E) as a function of temperature in an applied field of $\mu_0 H = 3$ mT. The onset temperature T_{so} is defined as the temperatures where the linearly extrapolated low- and high-temperature data points intersect (see Fig. 3).

The values of the static spin-stripe order temperature T_{so} and the SC transition temperatures T_{c1} and T_{c2} for $La_{2-x}Ba_xCuO_4$ ($0.11 \leqslant x \leqslant 0.17$), obtained from susceptibility, ZF μSR, and WTF μSR experiments are summarised in Fig. 4. It is important to note that the values of T_{so} determined from the WTF-μSR experiments are the same as the ones determined

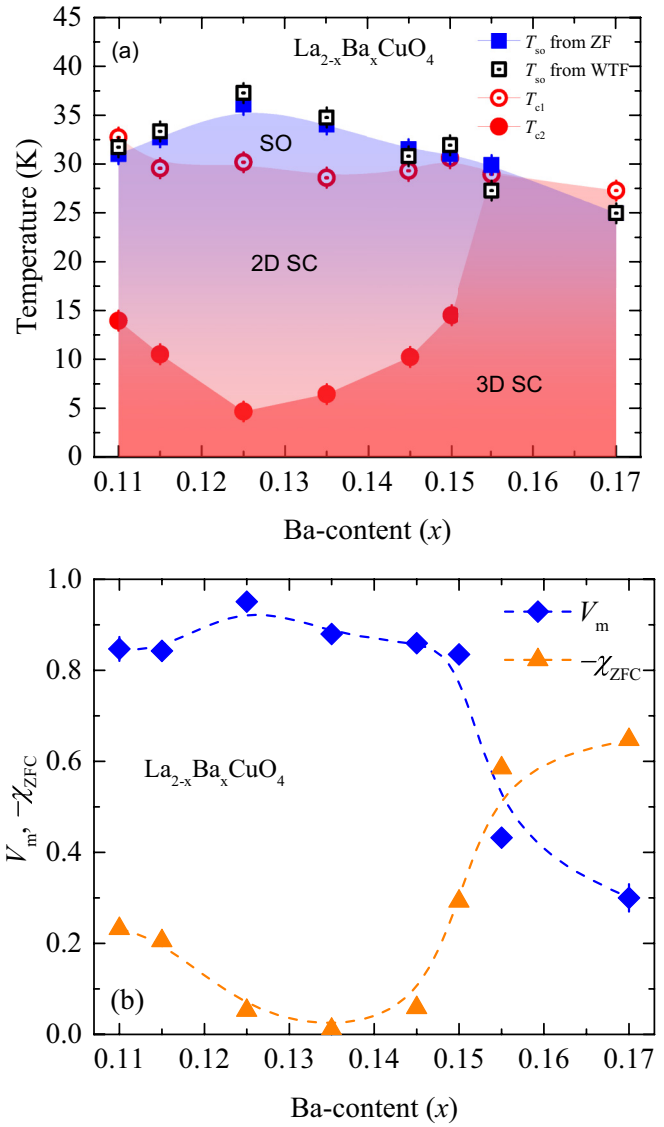

FIG. 4. (a) The static spin-stripe order temperature T_{so} and the SC transition temperatures T_{c1} and T_{c2} as a function of Ba-content x in $La_{2-x}Ba_xCuO_4$, as determined from ZF-μSR, WTF-μSR, and magnetization experiments. (b) The magnetic volume fraction V_m and the diamagnetic susceptibility χ_{ZFC} as a function of Ba content x in $La_{2-x}Ba_xCuO_4$.

from the ZF-μSR experiments. This indicates that the WTF-μSR measurements give reliable values for T_{so}. So this method will be used to extract T_{so} for the samples $x = 0.155$ and 0.17 under pressure. T_{c2} shows a local minimum close to 1/8 doping, which is consistent with a previous report [8]. On the other hand, T_{c1} exhibits a high value $\sim$30 K for all investigated x. Note that for $x = 0.155$ and 0.17 $T_{c1} = T_{c2}$, thus for these two samples the SC transition temperature will be denoted as T_c throughout the paper. Remarkably, the transition temperatures T_{c1} and T_{so} have very similar values throughout the phase diagram, giving strong evidence for a cooperative development of static order and SC pairing correlations in the striped cuprate system $La_{2-x}Ba_xCuO_4$.

Figure 4(b) demonstrates an antagonistic doping dependence of the magnetic volume fraction V_m and the diamagnetic susceptibility χ_{ZFC}. As it will be shown below for the $x = 0.155$ sample, χ_{ZFC}(5 K) scales with the magnetic penetration depth $\lambda^{-2}(T = 0)$ (Shoenberg model). However, a doping induced change of χ_{ZFC}(5 K) may be related not only to a change of λ but also to a change of the SC volume fraction or combination of both. Since λ was not measured for whole series of samples $La_{2-x}Ba_xCuO_4$, we cannot conclude which one of these two effects plays the dominant role in the observed changes of χ_{ZFC}(5 K). According to the results presented above the samples $x = 0.155$ and 0.17 exhibit both well defined bulk superconductivity and static spin-stripe order. Furthermore, at ambient pressure static magnetism and superconductivity set in at approximately the same temperature $T_{so} \simeq T_c = 30.5(5)$ and $T_{so} \simeq T_c = 27.5(5)$ for LBCO-0.155 and LBCO-0.17, respectively. Therefore we performed investigations of the stripe order and superconductivity in these systems under pressure. The obtained results will be presented and discussed below.

B. High-pressure magnetic susceptibility data

Figure 5 shows the temperature dependence of the zero-field-cooled (ZFC) magnetic susceptibility χ_{ZFC} for LBCO-0.155 recorded in a magnetic field of $\mu_0 H = 0.5$ mT for selected hydrostatic pressures after substraction of the background signal from the empty pressure cell. At ambient pressure superconductivity sets in at $T_c = 30.5(5)$ K [see Fig. 1(g)]. With increasing pressure T_c increases with 3 K/GPa up to $p \simeq 1.5$ GPa where it reaches $T_c = 35(1)$ K, then it stays constant up to $p = 2.2$ GPa. For $p > 2.2$ GPa, T_c tends to decrease up to the highest pressure of $p = 3.1$ GPa. The pressure dependence of T_c is displayed in Fig. 14 and will be discussed later. The magnitude of χ_{ZFC} at the base temperature ($T = 5$ K) is also enhanced with applied pressure (see Fig. 5) from $|\chi_{ZFC}| = 0.45(5)$ at $p = 0$ GPa to the saturated value $|\chi_{ZFC}| = 0.65(5)$ at $p \simeq 1$ GPa. It was found that χ_{ZFC}(5 K) scales with $\lambda^{-2}(T = 0)$ (λ is the magnetic

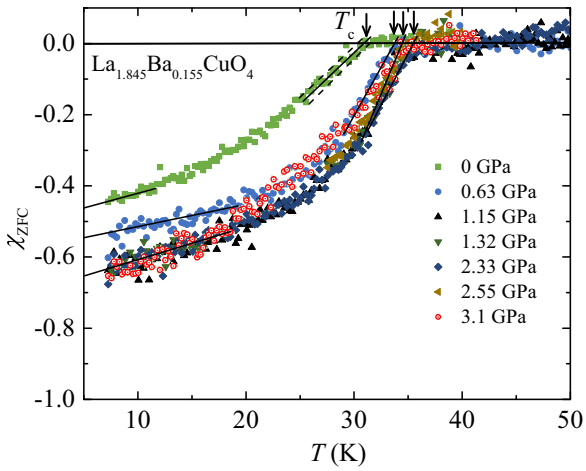

FIG. 5. Diamagnetic susceptibility χ_{ZFC} of LBCO-0.155 as a function of temperature and pressure. The dependence was measured at ambient and at various applied hydrostatic pressures in a magnetic field of $\mu_0 H = 0.5$ mT. The arrows denote the superconducting transition temperature T_c.

penetration depth) as determined from TF-μSR experiments [see Fig. 15(a)]. According to the Shoenberg model [33], χ_{ZFC} in a granular sample is expected to scale with λ^{-2} due to the penetration of the magnetic field on a distance λ from the surface of each individual grain. Since we did not measure the grain size for this particular sample it is difficult to judge whether the Schoenberg model applies here and whether the increase of $|\chi_{ZFC}|$ is caused by an increase of λ^{-2}. A pressure induced increase of $|\chi_{ZFC}|$ can be related either to an increase of the SC volume fraction or to a change of λ or a combination of both. For all these reasons, it is not possible to extract an absolute value for the SC volume fraction. In LBCO-0.17 superconductivity sets in at $T_c = 27.5(5)$ K at ambient pressure [see Fig. 1(h)]. Note that for this sample the magnetic susceptibility was not measured under pressure. The SC properties under pressure, i.e., T_c as well as the superfluid density, were determined by TF μSR experiments (Sec. V D).

C. Static magnetism as a function of pressure in LBCO-0.155 and LBCO-0.17

Figures 6(a) and 6(b) show representative ZF μSR time spectra for a polycrystalline LBCO-0.155 sample, recorded at 5 K at ambient and at selected hydrostatic pressures up to $p = 2.2$ GPa. For ambient pressure, the ZF μSR time spectrum taken at 40 K is also shown in Fig. 6(a). At $T = 40$ K, no muon spin precession, but only a very weak depolarization of the μSR signal is observed [see Fig. 6(a)]. This weak depolarization and its Gaussian functional form are typical for a paramagnetic material and reflect the occurrence of a small Gaussian Kubo-Toyabe depolarization, originating from the interaction of the muon spin with randomly oriented nuclear magnetic moments. At $T \approx 5$ K, damped oscillations due to muon-spin precession in internal magnetic fields are observed at pressures up to $p = 0.67$ GPa. The μSR time spectra are well described by a zeroth-order Bessel function which is characteristic for an incommensurate spin density wave [Eq. (2)], suggesting the presence of long-range static spin-stripe order in LBCO-0.155 [9,30] up to $p = 0.67$ GPa. The oscillation frequency is nearly pressure independent. On the other hand, for $p \leqslant 0.67$ GPa, the amplitude of this oscillation gradually decreases with increasing pressure, indicating a reduction of the magnetic volume fraction under pressure in agreement with our previous paper [25]. In the pressure range 0.83 GPa $\leqslant p \leqslant 2.2$ GPa, instead of the oscillatory behavior seen in the spin-ordered state for $p \leqslant 0.67$ GPa, a rapidly depolarizing ZF-μSR time spectrum is observed [see Fig. 6(b)]. For clarity, Fig. 6(b) shows ZF-μSR time spectra after subtraction of the pressure cell signal from the total one (Appendix and Fig. 17). One can clearly see a rapidly depolarizing component visible at early times ($\leqslant$0.25 μs) of the spectra, while the nonmagnetic part of the sample gives rise to a slow relaxation component, apparent at longer times (>0.25 μs). The fast depolarization of the μSR signal (with no trace of an oscillation) could be either due to a broad distribution of static fields, and/or to strongly fluctuating magnetic moments. To discriminate between these two possibilities, we have performed decoupling experiments in longitudinal fields. Figure 7(a) shows $A_{tot}(t)$ measured at 5 K and $p = 0.83$ GPa with different magnetic fields applied along the initial direction of the muon spin polarization. These

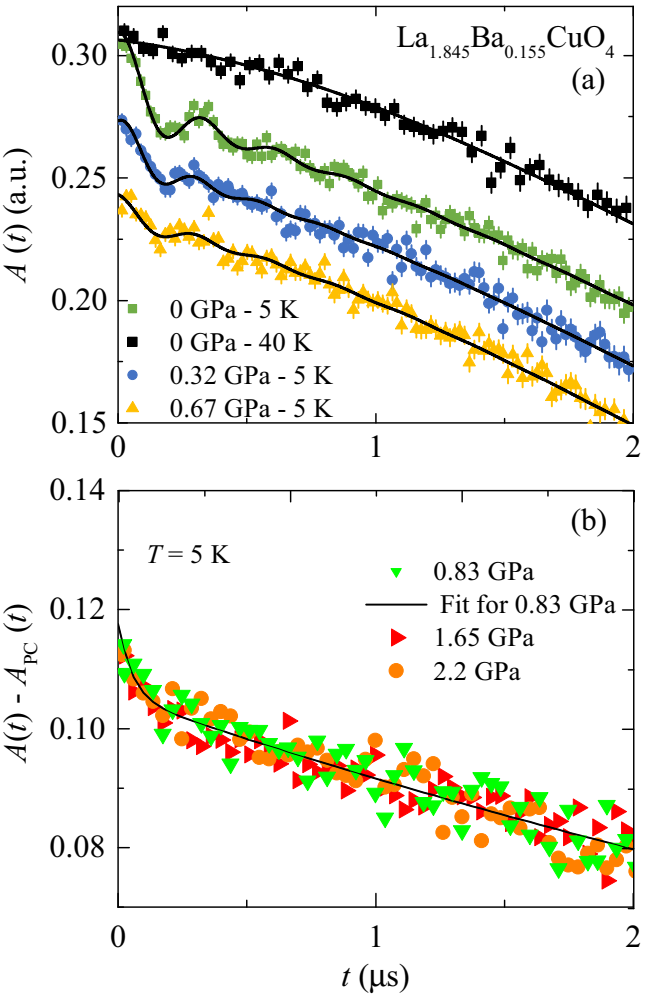

FIG. 6. (a) ZF μSR time spectra $A(t)$ for LBCO-0.155 recorded at 5 K in the pressure range of $0 \leqslant p \leqslant 0.67$ GPa. The μSR time spectrum at 40 K for 0 GPa is also shown. (b) μSR time spectra for LBCO-0.155 after subtracting the pressure cell contribution from the total signal, $A_S(t) = A(t) - A_{PC}(t)$, recorded at 5 K in the pressure range $0.83 \leqslant p \leqslant 2.2$ GPa. The solid lines represent fits to the data by means of Eq. (1).

experiments show that at modest external fields between 25 and 50 mT (of the order of the internal quasistatic fields) the muon-spin relaxation is substantially suppressed. This means that the muon spins are fully decoupled from the internal magnetic fields, demonstrating that the weak internal fields are static rather than dynamic, supporting the quasistatic origin of the fast muon-spin depolarization for $p > 0.83$ GPa. The rapid exponential relaxation of the ZF-μSR signal implies that the spread of the local magnetic field must be fairly large. A possible explanation may be that the spatially inhomogeneous magnetic state seen by μSR is strongly disordered. This indicates that in LBCO-0.155 the pressure causes a transition from the long-range static spin-ordered to a strongly disordered state at $p \sim 1$ GPa. Figure 7(b) shows A_{tot}(t) recorded in a longitudinal field (LF) of 10 mT at various temperatures. It clearly shows that the muon-spin relaxation increases below about 35 K, providing further evidence for quasistatic magnetic order in LBCO-0.155 at $p = 0.83$ GPa. For LBCO-0.17 the

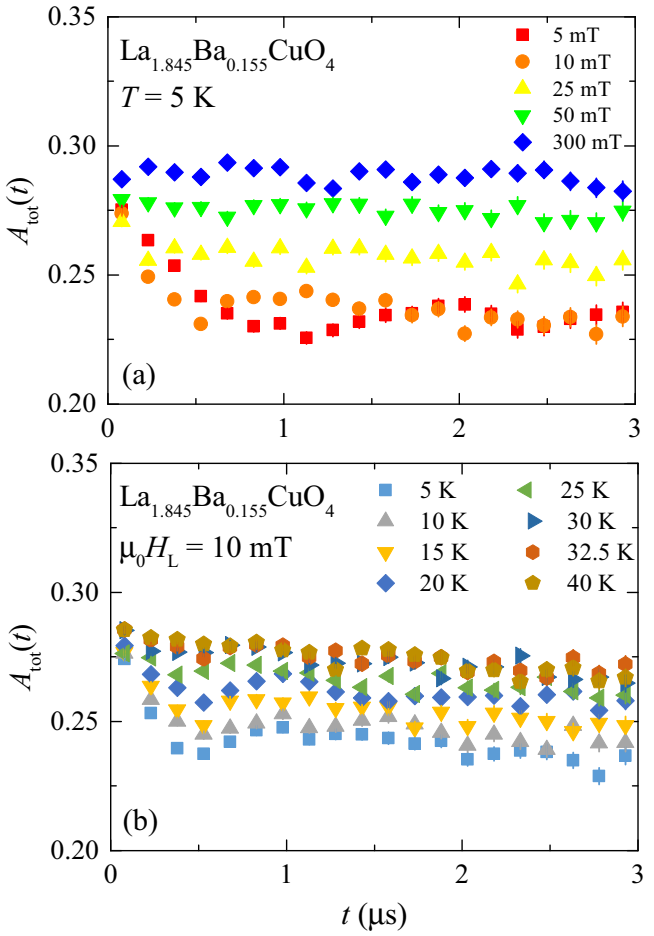

FIG. 7. (a) LF-μSR time spectra $A_{tot}(t)$ of LBCO-0.155 recorded at $T = 5$ K and $p = 0.83$ GPa with different magnetic fields applied along the initial direction of the muon-spin polarization. (b) LF-μSR spectra $A_{tot}(t)$ of LBCO-0.155 taken in an applied longitudinal field of $\mu_0 H_L = 10$ mT for various temperatures (5 K $\leqslant T \leqslant$ 40 K).

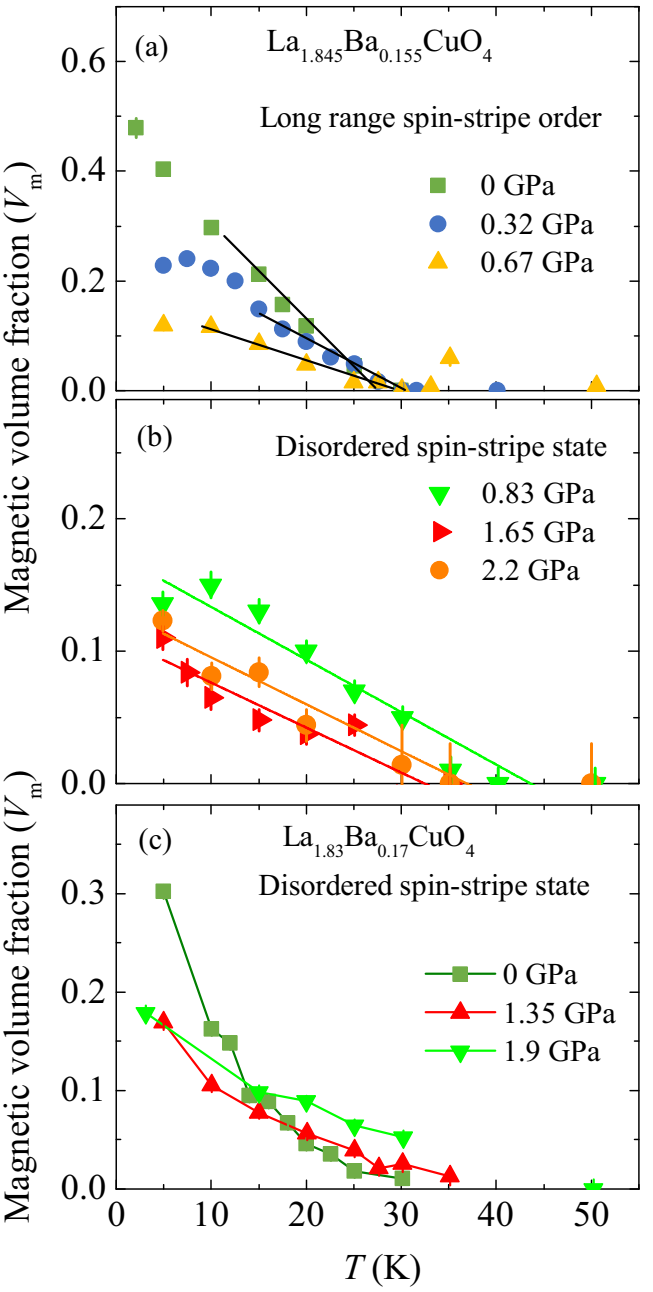

FIG. 8. Temperature dependence of the magnetic volume fraction V_m in LBCO-0.155 at various hydrostatic pressures: (a) $0 \leqslant p \leqslant 0.67$ GPa: pressure range where a well defined muon spin precession is observed, and (b) $0.83 \leqslant p \leqslant 2.2$ GPa: pressure range where only a fast depolarization of the μSR time signal is observed. (c) Temperature dependence of V_m in LBCO-0.17 at various hydrostatic pressures. The solid lines are guides to the eye.

μSR precession is strongly damped and no coherent precession signal is observed at any pressure, indicating the presence of a disordered magnetic state in this system even at ambient pressure (Fig. 2).

Next, we present the pressure dependencies of the magnetic volume fraction V_m and the static spin-stripe order temperature T_{so} in LBCO-0.155 and LBCO-0.17, extracted from the ZF-μSR data. Figures 8(a) and 8(b) show the temperature dependence of V_m for LBCO-0.155 in the pressure range of $0 \leqslant p \leqslant 0.67$ GPa (long-range spin-stripe ordered state) and 0.83 GPa $\leqslant p \leqslant 2.2$ GPa (disordered spin-stripe state), respectively. Below $T_{so} \simeq 30$ K, V_m increases progressively with decreasing temperature, and acquires nearly 50 % at ambient pressure at the base temperature $T = 2$ K. At low temperature, V_m significantly decreases with increasing pressure, reaching about 15% at 0.67 GPa [see Fig. 8(a)]. On the other hand, V_m of the disordered spin-stripe state observed in the pressure range 0.83 GPa $\leqslant p \leqslant 2.2$ GPa exhibits a much weaker pressure dependence and reaches about 15% at $T = 5$ K [see Fig. 8(b)]. Figure 8(c) shows the temperature dependence of V_m for LBCO-0.17 in the pressure range of $0 \leqslant p \leqslant 1.9$ GPa (disordered spin-stripe state). Below $T_{so} \simeq 25$ K, V_m increases progressively with decreasing temperature, and reaches nearly 30% at ambient pressure at $T = 5$ K.

In order to accurately determine T_{so} from μSR, TF-μSR experiments in a weak transverse field were carried out. Figures 9(a) and 9(b) show the TF-μSR asymmetry A_S' of LBCO-0.155 and LBCO-0.17 extracted from the μSR spectra (following the procedure given in II.E) as a function of temperature for ambient and selected applied pressures in an

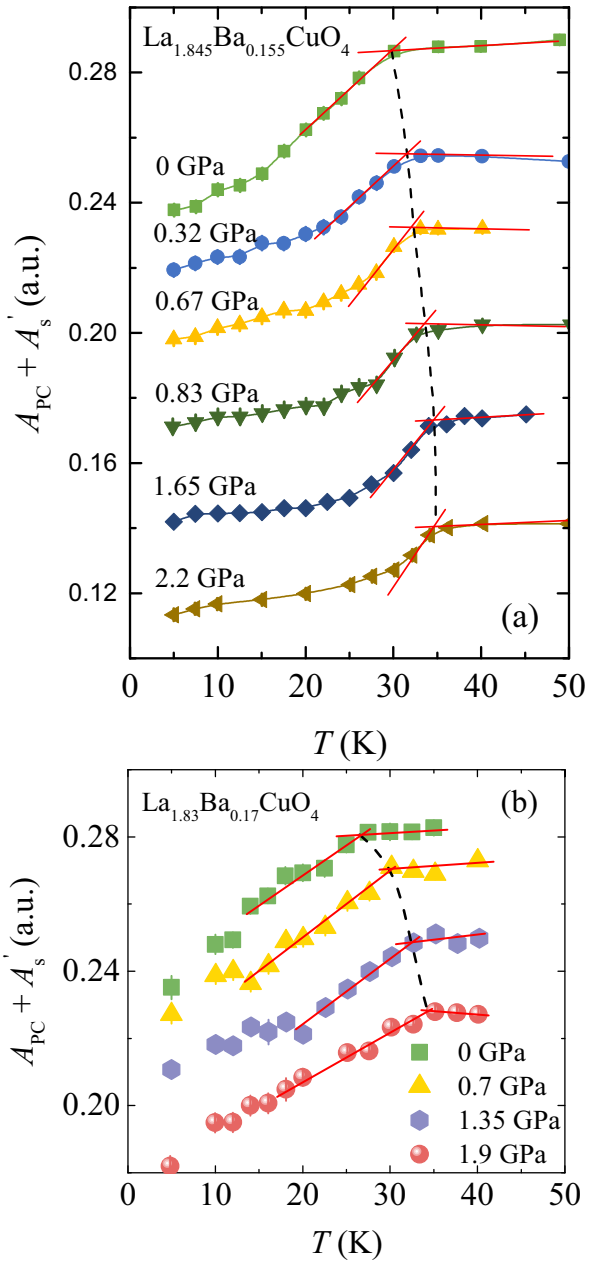

FIG. 9. TF asymmetry $A_S^{'}$ for LBCO-0.155 (a) and LBCO-0.17 (b) as a function of temperature for ambient and selected applied pressures in an applied field of $\mu_0 H = 3$ mT. The onset temperature to the magnetically ordered state T_{so} is defined as the temperatures where the linearly extrapolated low- and high-temperature data points intersect (indicated by the straight lines). The solid curves are guides to the eye.

applied field of $\mu_0 H = 3$ mT. For $p = 0$ GPa and $T > 30$ K for LBCO-0.155 ($T > 27$ K for LBCO-0.17), $A^{'}$ reaches the maximum value, indicating that the whole sample is in the paramagnetic state, with all the muon spins precessing in the applied magnetic field. Below 30 K (27 K), $A^{'}$ continuously decreases with decreasing temperature. The reduction of $A^{'}$ signals the appearance of magnetic order in the spin-stripe phase, where the muon spins experience a local magnetic field larger than the applied magnetic field. As a result, the fraction of muons in the paramagnetic state decreases. The onset temperature T_{so} is defined as the temperatures where the linearly extrapolated low- and high-temperature data points intersect [see Figs. 9(a) and 9(b)], yielding $T_{so} = 30(1)$ and 27(1) K at $p = 0$ GPa, for LBCO-0.155 and LBCO-0.17, respectively. Note that this agrees with ZF-μSR results. By applying pressure T_{so} in LBCO-0.155 first increases with increasing pressure, reaching $T_{so} = 35(1)$ K at 1.65 GPa, and then tends to saturate as shown in Fig. 14(a). In LBCO-0.17, T_{so} also increases monotonously with increasing pressure, reaching $T_{so} \simeq 34$ K at $p = 1.9$ GPa [see Fig. 14(b)]. Note that in LBCO-0.15 and LBCO-0.17 $T_c(p) \simeq T_{so}(p)$ at all applied pressures up to the maximum applied pressure of 2.2 and 1.9 GPa, respectively. This is a remarkable finding.

D. Probing the vortex state in LBCO-0.155 and LBCO-0.17 as a function of pressure

In the following, we present the pressure dependence of the μSR relaxation rate σ_{sc} for LBCO-0.15 and LBCO-0.17, which is a measure of the superfluid density ρ_s according to the relation: $\sigma_{sc} \propto \rho_s \equiv n_s/m^*$, where n_s is the SC carrier density, and m^* is the effective mass of the SC carriers.

Figure 10(a) exhibits TF-μSR-time spectra for LBCO-0.155, measured at the maximum applied pressure $p = 2.2$ GPa in 10 mT. Spectra above (45 K) and below (5 K) the SC transition temperature T_c are shown. Above T_c the oscillations show a small relaxation due to the random local fields from the nuclear magnetic moments. Below T_c the relaxation rate strongly increases with decreasing temperature due to the presence of a nonuniform local magnetic field distribution as a result of the formation of a flux-line lattice (FLL) in the SC state. Figure 10(b) shows the Fourier transforms (FT) of the μSR time spectra shown in Fig. 10(a). At $T = 5$ K, the narrow signal around $\mu_0 H_{ext} = 10$ mT originates from the pressure cell, while the broad signal with a first moment $\mu_0 H_{int} < \mu_0 H_{ext}$, marked by the orange solid arrow in Fig. 10(b), arises from the SC sample.

The TF μSR data were analyzed by using the following functional form [31]:

$$P(t) = A_{s1} \exp\left[-\frac{(\sigma_{sc}^2 + \sigma_{nm}^2)t^2}{2}\right] \cos(\gamma_\mu B_{int,s} t + \varphi) + A_{s2}\left[\frac{2}{3}e^{-\lambda_T t} + \frac{1}{3}e^{-\lambda_L t}\right] + A_{pc} \exp\left[-\frac{\sigma_{pc}^2 t^2}{2}\right] \cos(\gamma_\mu B_{int,pc} t + \varphi). \quad (4)$$

Here, A_{s1}, A_{s2}, and A_{pc} denote the initial asymmetries of the sample and the pressure cell, respectively. A_{s1} and A_{s2} are proportional to the SC and magnetic fractions of the sample, respectively. $\gamma/(2\pi) \simeq 135.5$ MHz/T is the muon gyromagnetic ratio, φ is the initial phase of the muon-spin ensemble. $B_{int,s}$ and $B_{int,pc}$ represent the local magnetic fields, probed by the muons, stopped in the sample and the pressure cell, respectively. The relaxation rates σ_{sc} and σ_{nm} characterize the damping due to the formation of the vortex lattice in the SC state and of the nuclear magnetic dipolar contribution, respectively. In the analysis, σ_{nm} was assumed to be constant over the entire temperature range and was

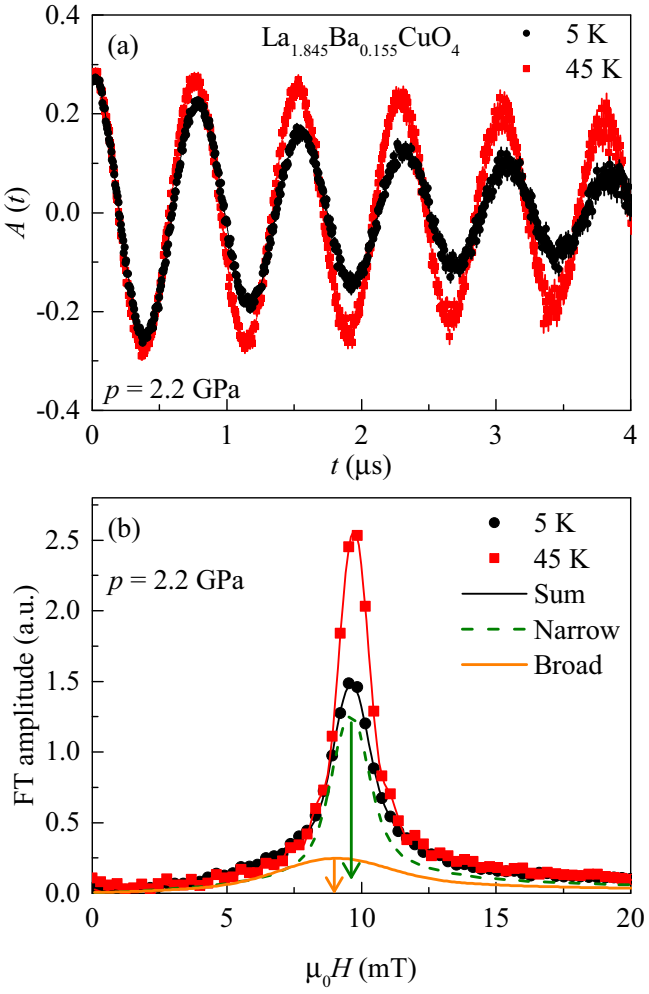

FIG. 10. Transverse-field (TF) μSR time spectra $A(t)$ (a) and the corresponding Fourier transforms (FTs) (b) of LBCO-0.155. The spectra were obtained at $p = 2.2$ GPa above (45 K) and below (5 K) T_c (after field cooling the sample from above T_c). The solid lines in panel (a) represent fits to the data by means of Eq. (4). The solid lines in panel (b) are the FTs of the fitted time spectra. The arrows indicate the first moments for the signals of the pressure cell (green) and the sample (orange), respectively.

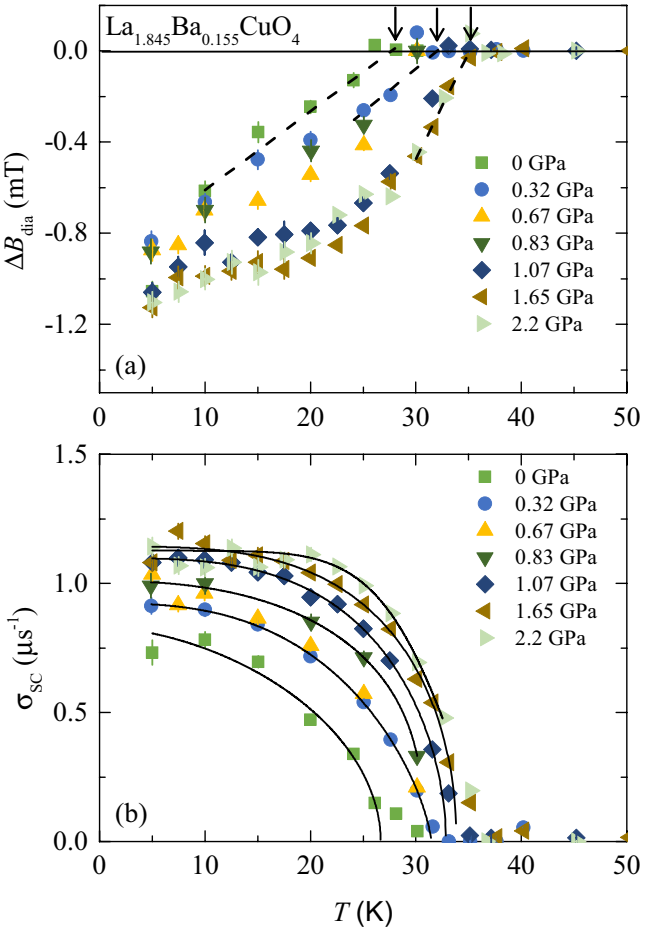

FIG. 11. Diamagnetic shift ΔB_{dia} (a) and μSR relaxation rate σ_{sc} (b) of LBCO-0.155 as a function of temperature at various pressures. (a) The definition of the diamagnetic shift ΔB_{dia} is given in the text. The arrows denote T_c for $p = 0, 0.32$, and 2.2 GPa. (b) μSR relaxation rate σ_{sc} measured in a magnetic field of $\mu_0 H = 10$ mT. The solid lines represent fits of the data to the power law described in the text.

fixed to the value obtained above T_c, where only nuclear magnetic moments contribute to the μSR relaxation rate σ. The Gaussian relaxation rate σ_{pc} reflects the depolarization due to the nuclear magnetism of the pressure cell. It can be seen from the FTs shown in Fig. 10(b) that the width of the pressure cell signal slightly increases below T_c. As shown previously [34], this is due to the stray fields in the pressure cell arising from the diamagnetism of the SC sample, leading to a temperature dependent σ_{pc} below T_c. In order to consider this influence, we assume a linear coupling between σ_{pc} and the field shift of the internal magnetic field in the SC state: $\sigma_{pc}(T) = \sigma_{pc}(T > T_c) + C(T)(\mu_0 H_{int,NS} - \mu_0 H_{int,SC})$, where $\sigma_{pc}(T > T_c) = 0.35\ \mu s^{-1}$ is the temperature independent Gaussian relaxation rate. $\mu_0 H_{int,NS}$ and $\mu_0 H_{int,SC}$ are the internal magnetic fields measured in the normal and in the SC state, respectively. As indicated by the solid lines in Figs. 10(a) and 10(b), the μSR time spectra are well described by Eq. (4). The solid lines in panel (b) are the FTs of the fitted curves shown in Fig. 10(a). The model used describes the data rather well.

Below T_c, a large diamagnetic shift of $\mu_0 H_{int}$ experienced by the muons is observed at all applied pressures. This is evident in Fig. 11(a) where we plot the temperature dependence of the diamagnetic shift $\Delta B_{dia} = \mu_0[H_{int,SC} - H_{int,NS}]$ for LBCO-0.155 at various pressures, where $\mu_0 H_{int,SC}$ denotes the internal field measured in the SC state and $\mu_0 H_{int,NS}$ the internal field measured in the normal state at 45 K. Note that $\mu_0 H_{int,NS}$ is temperature independent. The SC transition temperature T_c is determined from the intercept of the linearly extrapolated ΔB_{dia} curve and its zero line [we used the same criterium for the determination of T_c from $\Delta B_{dia}(T)$ as from the susceptibility data $\chi_{ZFC}(T)$ presented above], yielding $T_c = 28.3$ (5) K for $p = 0$ GPa. This value of T_c is in fair agreement with $T_c = 30.5(9)$ K obtained from the susceptibility data presented above. With increasing pressure T_c increases and reaches $T_c \simeq 35$ K at $p = 1.07$ GPa. Above $p = 1.07$ GPa, T_c seems to saturate, which is in perfect agreement with the high-pressure magnetization data (see

Fig. 5). Application of pressure causes an enhancement of the diamagnetic shift, which reaches its saturation value above $p = 1.07$ GPa.

The temperature dependence of the μSR relaxation rate σ_{sc} of LBCO-0.155 in the SC state at selected pressures is shown in Fig. 11(b). The μSR relaxation rate σ_{sc} is proportional to the second moment of local magnetic field distribution present in the sample. Below T_c the relaxation rate σ_{sc} starts to increase from zero with decreasing temperature due to the formation of the FLL. The solid curves in Fig. 11(b) are fits of the data to the power law $\sigma_{sc}(T) = \sigma_{sc}(0)[1 - (T/T_c)^{\gamma}]^{\delta}$, where $\sigma_{sc}(0)$ is the zero-temperature value of σ_{sc}. γ and δ are phenomenological exponents. The low-temperature value $\sigma_{sc}(0)$ increases under pressure by about 40% from $p = 0$ GPa to $p = 1.07$ GPa and saturates above [see Fig. 15(a)]. Note that the saturation of the diamagnetic shift ΔB_{dia} [Fig. 11(a)], diamagnetic susceptibility χ_{ZFC} [Fig. 15(a)] as well as of $\sigma_{sc}(0)$ [Fig. 15(a)] takes place at the same applied pressure $p^* \simeq 1$ GPa.

Figure 12 shows the temperature dependence of the diamagnetic shift ΔB_{dia} (a) and the μSR relaxation rate

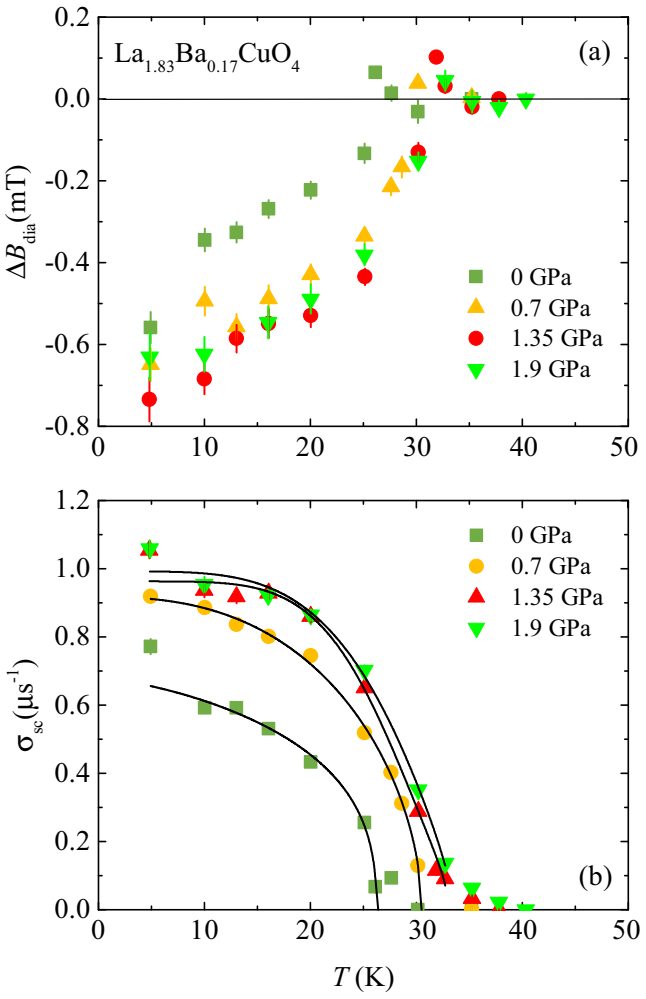

FIG. 12. Diamagnetic shift ΔB_{dia} (a) and μSR relaxation rate σ_{sc} (b) of LBCO-0.17 as a function of temperature at various pressures. σ_{sc} is measured in a magnetic field of $\mu_0 H = 10$ mT. The solid lines represent fits of the data to the power law described in the text.

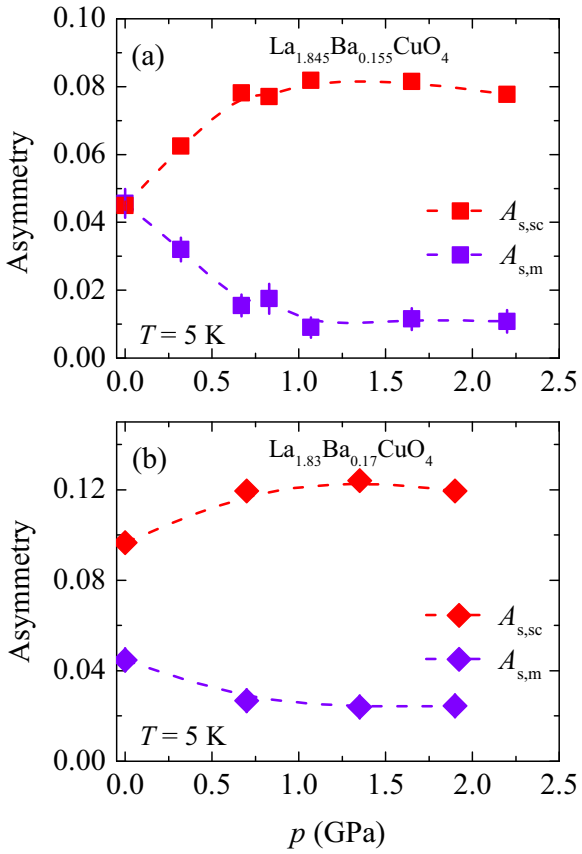

FIG. 13. Pressure dependence of the asymmetries $A_{s,sc}$ and $A_{s,m}$ of LBCO-0.17 (a) and LBCO-0.155 (b) at $T = 5$ K, corresponding to the SC and the magnetic parts of the sample.

σ_{sc} (b) of LBCO-0.177. Application of pressure causes an enhancement of the diamagnetic shift. The low-temperature value $\sigma_{sc}(0)$ increases strongly under pressure up to 0.7 GPa, and then a smooth increase is observed up to the highest appled pressure of $p = 1.9$ GPa [see Fig. 15(b)]. The overall increase of $\sigma_{sc}(0)$ is about 40%, i.e., same as observed for LBCO-0.155.

In Figs. 13(a) and 13(b), the asymmetries $A_{s,sc}$ and $A_{s,m}$, which are proportional to the SC and the magnetic fractions of the sample, respectively, are plotted as a function of pressure for LBCO-0.155 and LBCO-0.17. An increase of $A_{s,sc}$ and a simultaneous decrease of $A_{s,m}$ are observed upon increasing the pressure to $p^* = 1.07$ and 0.7 GPa, for LBCO-0.155 and LBCO-0.17, respectively. However, above p^* both saturate. This is in excellent agreement with the observed pressure dependence of the diamagnetic moment, obtained from the magnetization experiments [see Fig. 15(a)] and the magnetic volume fraction, extracted from the ZF-μSR experiments [see Figs. 15(a) and 15(b)].

IV. DISCUSSION

In order to compare the influence of pressure on the SC and magnetic properties of LBCO-0.155 and LBCO-0.17, the pressure dependencies of the magnetic transition temperature T_{so}, the SC transition temperature T_c, and the magnetic volume fraction V_m as well as the μSR relaxation rate

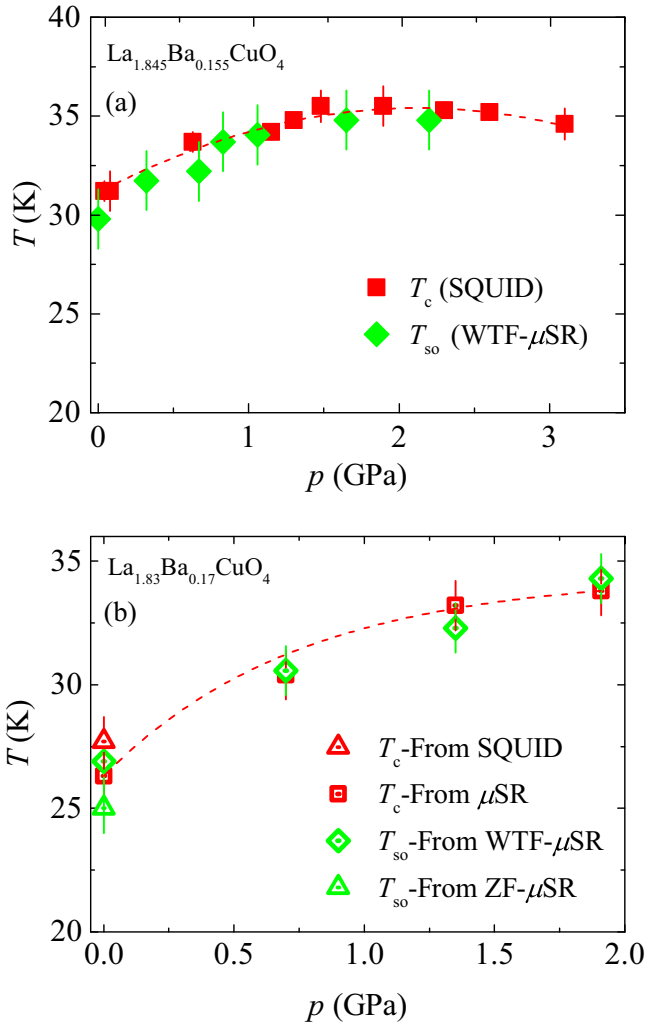

FIG. 14. The superconducting transition temperature T_c and the magnetic ordering temperature T_{so} of LBCO-0.155 (a) and LBCO-0.17 (b), obtained from dc susceptibility and μSR experiments, are plotted as a function of pressure.

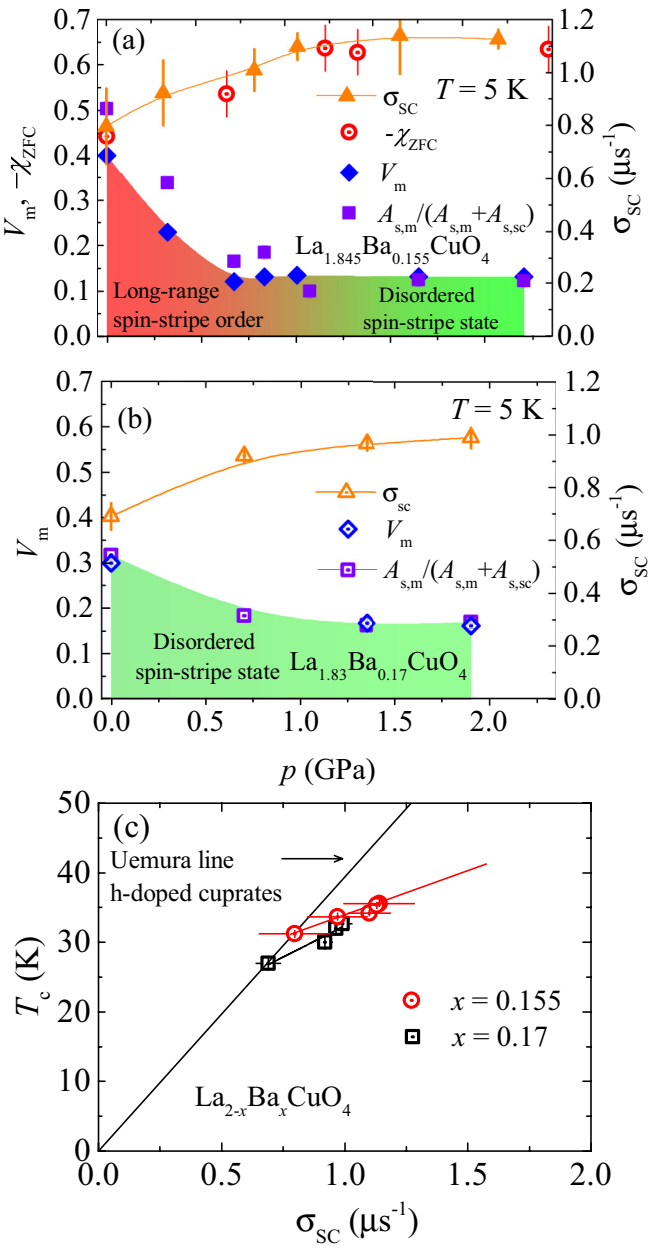

FIG. 15. (a) Pressure dependence of the μSR relaxation rate σ_{sc}, the diamagnetic susceptibility $-\chi_{ZFC}$, the magnetic volume fraction V_m and the quantity $A_{s,m}/(A_{s,m}+A_{s,sc})$ of LBCO-0.155 (a) and LBCO-0.17 (b) taken at 5 K. The solid lines are the guides to the eye. The long-range spin-stripe order and the disordered spin-stripe state are marked by different colors. (c) Uemura plot [T_c vs $\sigma_{sc}(0)$] for LBCO-0.155 and LBCO-0.17 at zero and applied pressure up to 2.2 and 1.9 GPa, respectively. The Uemura relation observed for underdoped cuprates is represented by the solid line for hole doping. The solid red and black lines represent linear fits of the data.

σ_{sc} are plotted in Figs. 14(a), 15(a) and Figs. 14(b), 15(b) for LBCO-0.155 and LBCO-0.17, respectively. In addition, the quantity $A_{s,m}/(A_{s,m}+A_{s,sc})$ is plotted for both samples [Figs. 15(a) and 15(b)].

The most essential findings of the present work are the following: (1) T_c and T_{so} have very similar values at all applied pressures as shown in Figs. 14(a) and 14(b). For LBCO-0.155 both increase up to $\simeq$35(1) K at $p \simeq 1.5$ GPa and are nearly constant at higher pressures up to $p \simeq 2.2$ GPa. For LBCO-0.17, T_c and T_{so} increase up to $\simeq$34(1) K at the maximum pressure $p \simeq 1.9$ GPa. (2) In LBCO-0.155, pressure causes a transition from the long-range static spin-stripe ordered ($0 \leqslant p \leqslant 0.67$ GPa) to a strongly disordered ($p \geqslant 0.83$ GPa) spin-stripe state [see Fig. 15(a)]. LBCO-0.17 exhibits a disordered magnetic state at ambient as well as at all applied pressures [see Fig. 15(b)].

To our knowledge, this is the first experimental evidence of a similar pressure evolution of the SC and the magnetic transition temperatures and a pressure induced change of the magnetic state in the stripe phase of cuprates. In view of recent theoretical and experimental works [35], we interpreted the observed disordered state as evidence for glassy spin-stripe order. While the absence of long-range stripe order in the presence of disorder is inevitable in two dimensions, a new possible glassy state, the so-called spin-density-wave (SDW) glass state, has recently been proposed [35]. In this SDW glass phase, the spins are frozen in time, but the phase of the SDW is

randomly disordered in space. The spins retain a common axis along which they randomly point up or down (spin nematic order). In the present case, because pressure does not affect the impurity concentration, the high-pressure putative glassy state is most probably caused by a possible frustrated phase separation [36] between the SC and magnetic ground states in LBCO-0.155, as will be discussed below.

Besides the above results, other interesting findings evident from Figs. 15(a) and 15(b) include the strong increase of the superfluid density $\rho_s \propto \sigma_{sc}$ under pressure and the reduction of the magnetic volume fraction V_m under pressure for both LBCO-0.155 and LBCO-0.17, despite the fact that T_{so} increases with pressure. As shown in Fig. 15(a), the low-temperature ($T = 5$ K) value of $\sigma_{sc} \propto \rho_s$ in LBCO-0.155 increases with increasing pressure and reaches a constant value at $p \simeq 1$ GPa, which is $\simeq$35% larger than the one at $p = 0$ GPa. On the other hand, the magnetic volume fraction V_m at $T = 5$ K sharply decreases with pressure from $\simeq 40\%$ at ambient pressure to approximately 15% at $p = 0.83$ GPa. For $p > 0.83$ GPa, V_m remains nearly constant. As demonstrated in Fig. 15(b), LBCO-0.17 shows a similar pressure evolution of σ_{sc} and V_m, i.e., antagonistic pressure behavior between these two quantities. It is interesting to note that a similar relation was found between the superfluid density and the magnetic volume fraction in the related compound $La_{1.85-y}Eu_ySr_{0.15}CuO_4$ [37], where the tuning of the magnetic and SC properties was realized by rare-earth doping. To further elucidate the interplay between V_m and ρ_s, it is important to understand the origin for the pressure enhancement of ρ_s. The Uemura relation in HTSs reflects a remarkable correlation between T_c and the zero-temperature μSR relaxation rate $\sigma_{SC}(0) \propto 1/\lambda^2(0)$ for cuprate HTSs [38]. This relation T_c versus $\sigma(0)$, which seems to be generic for various families of cuprate HTSs, shows in the underdoped regime $T_c \propto \sigma(0)$ (Uemura line) [see Fig. 15(c)]. At higher doping, T_c saturates and becomes independent of $\sigma(0)$, and finally in the heavily overdoped regime T_c is suppressed. The initial linear form of the Uemura relation indicates that for these unconventional HTSs the ratio T_c/E_F (E_F is an effective Fermi energy) is up to two orders of magnitude larger than for conventional BCS superconductors. The Uemura relation for the present μSR pressure data of LBCO-0.155 and LBCO-0.17 are shown in Fig. 15(c). As indicated by the red and the black solid lines, the slope $S_p = (\delta T_c/\delta P)/(\delta\sigma_{sc}(0)/\delta P)$ is a factor of $\simeq 3$ and 2 smaller, for LBCO-0.155 and LBCO-0.17, respectively, than that expected from the Uemura line [38] with $S_U = (\delta T_c/\delta P)/(\delta\sigma_{sc}(0)/\delta P) \simeq 40$ K/μs. A similar substantial deviation from the Uemura line was also observed in previous pressure studies of $YBa_2Cu_3O_7$ [34] and $YBa_2Cu_4O_8$ [39,40] as well as in oxygen-isotope effect studies of various cuprate superconductors [41]. A slope which is smaller than that of the Uemura line implies that the increase of the superfluid density $\rho_s(0) \propto \sigma(0)$ is caused not only by an increase of the SC carrier density n_s, but very likely also by a decrease of the effective mass m^* of the SC carriers. This result together with the observed bulk superconductivity detected by high pressure susceptibility measurements and the similar onset of magnetism and superconductivity in LBCO-0.155 and LBCO-0.17 under pressure suggest that these systems organize themselves so as to minimize the overlap between magnetic and superconducting order parameters by intertwining with each other. This suggestion is also supported by the doping dependent studies, revealing the similar values of T_{so} and T_c in the series of $La_{2-x}Ba_xCuO_4$ samples at ambient pressure (see Fig. 4). This is consistent with the concept of a spatially modulated SC (PDW) state which may avoid the amplitude-modulated antiferromagnetic spin correlations by intertwining with them [18–20]. Within the scenario of the intertwined orders one may understand that $T_c(p) \simeq T_{so}(p)$ and the coexistence of the high-pressure magnetic disordered stripe state and bulk superconductivity. Moreover, it also shares the concept of phase separation, but on a short length scale. The frustrated phase separation [42] between the SC and the long-range magnetic ground states in LBCO-0.155 and LBCO-0.17 leading to a state that is inhomogeneous on an intermediate length scale would be a possible explanation for the antagonistic pressure behavior between V_m and ρ_s. This also means that the two coexisting phases are in microscopic proximity to each other.

Furthermore, one should note the similarities and differences between the pressure effects observed in the present systems LBCO-0.155 and LBCO-0.17 in comparison with LBCO-1/8 [25]. (1) At ambient pressure, a well defined bulk 3D SC transition with $T_c \simeq 30$ and $\simeq$25 K takes place in LBCO-0.155 and LBCO-0.17, respectively, while in polycrystalline LBCO-1/8 two SC transitions were observed [25,32], as discussed above. The first transition appears at $T_{c1} \simeq 30$ K to a quasi-2D SC phase and the second transition at $T_{c2} \simeq 5$ K corresponds to the transition to a 3D SC phase.

(2) T_c and T_{so} have very similar values for LBCO-0.155 and LBCO-0.17. Remarkably, the values of 2D T_{c1} and T_{so} are also very similar for LBCO-1/8.

(3) In the case of LBCO-0.155 and LBCO-0.17 strong positive pressure effects on both T_c and T_{so} with $T_c(p) \simeq T_{so}(p)$ are present. We also measured the pressure dependence of the T_{so} in a new LBCO-1/8 sample and we plot the values of T_{so} and T_c as a function of pressure in Fig. 16. It is interesting to

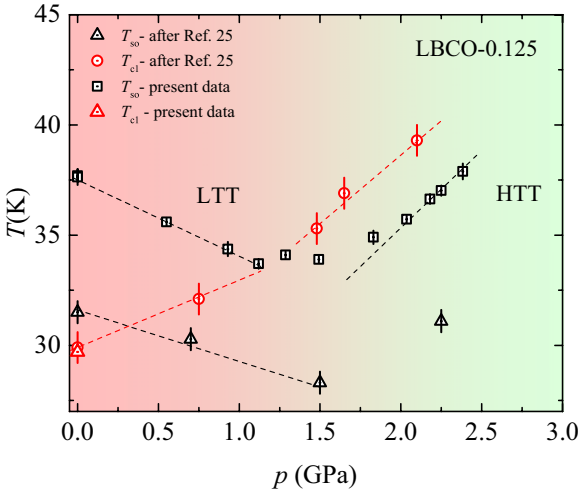

FIG. 16. Pressure dependence of T_{so} and T_{c1} for LBCO-1/8, taken from weak-transverse field μSR and magnetization data. The terms LTT and HTT stand for the low-temperature tetragonal and high-temperature tetragonal structural phases.

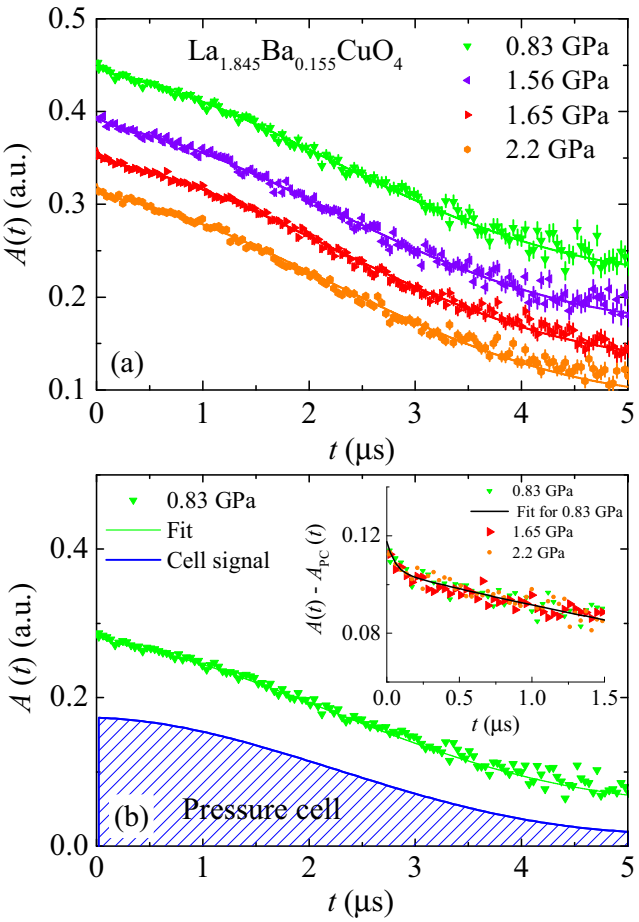

FIG. 17. Extracting the sample response from the total μSR signal for LBCO-0.155. (a) ZF μSR time spectra $A(t)$ for LBCO-0.155 measured in the pressure range 0.83 GPa $\leqslant p \leqslant$ 2.2 GPa recorded at $T = 5$ K. The solid lines represent fits to the data by means of Eqs. (1) and (2) of the main text. (b) For comparison, the total signal $A_{\rm tot}(t)$ (green triangles) together with the simulated pressure cell signal $A_{\rm PC}(t)$ (blue solid curve) is plotted for $p = 0.83$ GPa. The inset shows the difference between the total and the pressure cell signals $[A_S(t) = A(t) - A_{\rm PC}(t)]$ for part of the data ($t \leqslant 1.5$ μs) displayed in (b).

note that $dT_{\rm so}/dp$ and $dT_{\rm c}/dp$ have different signs for $p \leqslant 1.5$ GPa. For $p \geqslant 1.5$ GPa where the so-called low-temperature tetragonal (LTT) phase is suppressed [43,44], both $T_{\rm so}$ and $T_{\rm c}$ increase with increasing pressure with similar slopes. The values of $T_{\rm so}$ and $T_{\rm c1}$ do not really match ($T_{\rm so} < T_{\rm c1}$), but exhibit the same linear pressure dependence. Note that the values of $T_{\rm so}(p)$ for the new LBCO-1/8 sample are systematically higher that the ones reported previously [25]. This can be related to the slightly different preparation procedure of the two samples.

(4) For the samples with $x = 1/8$ and 0.155, we observed an antagonistic pressure dependence of the magnetic volume fraction and the diamagnetic susceptibility. In addition, in the samples with $x = 0.155$ and 0.17 an antagonistic pressure dependence of V_m and the superfluid density is observed. For the sample with $x = 0.155$, we were able to measure both the diamagnetic moment and the superfluid density, and we could compare the changes of both quantities under pressure. In the case of $x = 1/8$ only the diamagnetic moment was measured. We cannot extract reliable information about the superfluid density, since the magnetic fraction is nearly 100% at the ambient pressure. It is evident that the magnetic fraction decreases with increasing pressure, reaching 50% at the highest pressure, but it is not possible to follow the pressure evolution of the superfluid density. Probably, one can get a reliable SC response only close to the highest pressure. This means that we cannot definitely conclude which one of the two effects (increase of the SC volume fraction or increase of the penetration depth) plays the dominant role in the enhancement of $\chi_{\rm ZFC}$. Combining all the above mentioned experimental facts we may conclude that magnetism and superconductivity in $La_{2-x}Ba_xCuO_4$ are competing phenomena in terms of either volume fraction or superfluid density. In order to discriminate between these two scenarios further experimental and theoretical work is required. The fact that the 2D $T_{\rm c}$ for $x = 1/8$ as well as the bulk $T_{\rm c}$ for $x = 0.155$ and 0.17 have very similar values as $T_{\rm so}$, indicates that the order parameters of superconductivity and magnetism do not compete in terms of pairing strength. This suggests that the cooperative development of static order and SC pairing correlations in the striped cuprate system $La_{2-x}Ba_xCuO_4$ may be relevant near 1/8 doping as well as away from it.

The experimental facts listed above point to small differences between the pressure effects of LBCO-1/8 and LBCO-0.155/LBCO-0.17 with x far away from 1/8. To understand these differences between LBCO-1/8 and LBCO-0.155/LBCO-0.17, pressure effects on the structural properties of these systems are crucial. Note that already at ambient pressure the structural properties of these two systems are quite different. While in LBCO-1/8 a discontinuous transition from a low-temperature orthorhombic (LTO) to a LTT phase is observed [8,45], LBCO-0.155 and LBCO-0.17 exhibit no long-range LTT phase [8]. Different structural properties of these two systems may be a possible reason for the differences in the observed pressure effects.

V. CONCLUSIONS

In conclusion, static spin-stripe order and superconductivity were systematically studied in $La_{2-x}Ba_xCuO_4$ ($0.11 \leqslant x \leqslant 0.17$) at ambient pressure by means of magnetization and μSR experiments. We find that for all investigated doping concentrations x a substantial fraction of the sample is magnetic, and the 2D SC transition temperature $T_{\rm c1}$ and the static spin-stripe order temperature $T_{\rm so}$ have very similar values throughout the phase diagram. Moreover, magnetism and superconductivity were studied in LBCO-0.155 and LBCO-0.17 as a function of pressure up to $p \simeq 3.1$ GPa. Remarkably, it was found that in these systems the 3D SC transition temperature $T_{\rm c}$ and $T_{\rm so}$ have very similar values at all pressures, indicating the simultaneous appearance of static magnetic order and superconductivity at all applied pressures in LBCO-0.155 and LBC0-0.17. Antagonistic pressure behavior between the magnetic volume fraction V_m and the superfluid density $\rho_{\rm s}$ was observed in LBCO-0.155 and LBC0-0.17 under pressure up to $p \simeq 0.83$ and $\simeq$0.7 GPa, respectively, which was interpreted in terms of a frustrated phase separation scenario. Interestingly, in LBCO-0.155 for $p \geqslant 0.83$ GPa, where $\rho_{\rm s}$ reaches a constant value, long-range static spin-stripe order is not suppressed, but

is replaced by a disordered quasistatic magnetic state, which persists up to the highest applied pressure of $p = 2.2$ GPa. A disordered static magnetic state, observed in LBCO-0.17 at ambient pressure, also persists up to the highest applied pressure of $p = 1.9$ GPa. The present findings provide clear experimental evidence of a pressure induced change of the magnetic state as well as the same pressure evolution of the SC and the magnetic transition temperatures in the stripe phase of cuprates. These experimental results strongly suggest that static spin-stripe order and SC pairing correlations develop in a cooperative fashion in $La_{2-x}Ba_xCuO_4$.

ACKNOWLEDGMENTS

The μSR experiments were performed at the Swiss Muon Source (SμS) Paul Scherrer Insitute, Villigen, Switzerland. Z.G. thanks Y.J. Uemura, S.A. Kivelson, and J. Tranquada for helpful discussions. Z.G. thanks P.K. Biswas for his technical support during the experiments on Dolly μSR Instrument. Z.G. gratefully acknowledges the financial support by the Swiss National Science Foundation (SNFfellowship P2ZHP2_161980 and SNFGrant 200021_149486). A.S. acknowledges support from the SCOPES grant No. Z74Z0_160484. We further thank A. Schilling and F.v. Rohr for supporting the susceptibility measurements of LBCO-0.155 under pressure. Work in the Billinge group was supported by U.S. Department of Energy, Office of Science, Office of Basic Energy Sciences (DOE-BES) under Contract No. DE-SC00112704.

APPENDIX: EXTRACTING THE ZF-μSR SIGNAL OF LBCO-0.155 FOR $p \geqslant 0.83$ GPA

As already mentioned in the main text, in the pressure range $0.83\ \text{GPa} \leqslant p \leqslant 2.2$ GPa, instead of the oscillatory behavior seen in the spin-ordered state for $p < 0.67$ GPa, a rapidly depolarizing and a weak relaxing ZF-μSR signal are observed [see Fig. 17(a)]. The signal with weak exponential depolarization is affected by a substantial contribution arising from the pressure cell [see Fig. 17(b)], which is subtracted to extract the sample signal. The resulting μSR signal of the sample at $p = 0.83$ GPa is shown in the inset of Fig. 17(b).

[1] J. G. Bednorz and K. A. Müller, Z. Phys. B **64**, 189 (1986).
[2] A. R. Moodenbaugh, Y. Xu, M. Suenaga, T. J. Folkerts, and R. N. Shelton, Superconducting properties of $La_{2-x}Ba_xCuO_4$, Phys. Rev. B **38**, 4596 (1988).
[3] S. A. Kivelson, I. P. Bindloss, E. Fradkin, V. Oganesyan, J. M. Tranquada, A. Kapitulnik, and C. Howald, How to detect fluctuating stripes in the high-temperature superconductors, Rev. Mod. Phys. **75**, 1201 (2003).
[4] M. Vojta, Lattice symmetry breaking in cuprate superconductors: Stripes, nematics, and superconductivity, Adv. Phys. **58**, 699 (2009).
[5] J. M. Tranquada, B. J. Sternlieb, J. D. Axe, Y. Nakamura, and S. Uchida, Evidence for stripe correlations of spins and holes in copper oxide superconductors, Nature (London) **375**, 561 (1995).
[6] J. M. Tranquada, J. D. Axe, N. Ichikawa, Y. Nakamura, S. Uchida, and B. Nachumi, Neutron-scattering study of stripe-phase order of holes and spins in $La_{1.48}Nd_{0.4}Sr_{0.12}CuO_4$, Phys. Rev. B **54**, 7489 (1996).
[7] P. Abbamonte, A. Rusydi, S. Smadici, G. D. Gu, G. A. Sawatzky, and D. L. Feng, Spatially modulated 'Mottness' in $La_{2-x}Ba_xCuO_4$, Nat. Phys. **1**, 155 (2005).
[8] Hücker, M. v. Zimmermann, G. D. Gu, Z. J. Xu, J. S. Wen, Guangyong Xu, H. J. Kang, A. Zheludev, and J. M. Tranquada, Stripe order in superconducting $La_{2-x}Ba_xCuO_4$ ($0.095 \leqslant x \geqslant 0.155$), Phys. Rev. B **83**, 104506 (2011).
[9] G. M. Luke, L. P. Le, B. J. Sternlieb, W. D. Wu, Y. J. Uemura, J. H. Brewer, T. M. Riseman, S. Ishibashi, and S. Uchida, Static magnetic order in $La_{1.875}Ba_{0.125}CuO_4$, Physica C **185-189**, 1175 (1991).
[10] J. Arai, T. Ishiguro, T. Goko, S. Iigaya, K. Nishiyama, I. Watanabe, and K. Nagamine, J. Low Temp. Phys. **131**, 375 (2003).
[11] T. Wu, H. Mayaffre, S. Krämer, M. Horvatić, C. Berthier, W. N. Hardy, R. Liang, D. A. Bonn, and M. H. Julien, Magnetic-field-induced charge-stripe order in the high-temperature superconductor $YBa_2Cu_3O_y$, Nature (London) **477**, 191 (2011).
[12] Y. Kohsaka, C. Taylor, K. Fujita, A. Schmidt, C. Lupien, T. Hanaguri, M. Azuma, M. Takano, H. Eisaki, H. Takagi, S. Uchida, and J. C. Davis, An intrinsic bond-centered electronic glass with unidirectional domains in underdoped cuprates, Science **315**, 1380 (2007).
[13] J. M. Tranquada, Spins, stripes, and superconductivity in hole-doped cuprates, AIP Conf. Proc. **1550**, 114 (2013).
[14] J. M. Tranquada, G. D. Gu, M. Hücker, Q. Jie, H.-J. Kang, R. Klingeler, Q. Li, N. Tristan, J. S. Wen, G. Y. Xu, Z. J. Xu, J. Zhou, and M. v. Zimmermann, Evidence for unusual superconducting correlations coexisting with stripe order in $La_{1.875}Ba_{0.125}CuO_4$, Phys. Rev. B **78**, 174529 (2008).
[15] Q. Li, M. Hücker, G. D. Gu, A. M. Tsvelik, and J. M. Tranquada, Two-Dimensional Superconducting Fluctuations in Stripe-Ordered $La_{1.875}Ba_{0.125}CuO_4$, Phys. Rev. Lett. **99**, 067001 (2007).
[16] T. Valla, A. V. Fedorov, J. Lee, J. C. Davis, and G. D. Gu, The ground state of the pseudogap in cuprate superconductors, Science **314**, 1914 (2006).
[17] R.-H. He, K. Tanaka, S.-K. Mo, T. Sasagawa, M. Fujita, T. Adachi, N. Mannella, K. Yamada, Y. Koike, Z. Hussain, and Z.-X. Shen, Energy gaps in the failed high-T_c superconductor $La_{1.875}Ba_{0.125}CuO_4$, Nat. Phys. **5**, 119 (2009).
[18] E. Fradkin, S. A. Kivelson, and J. M. Tranquada, Colloquium: Theory of intertwined orders in high temperature superconductors, Rev. Mod. Phys. **87**, 457 (2015).
[19] A. Himeda, T. Kato, and M. Ogata, Stripe States with Spatially Oscillating d-Wave Superconductivity in the Two-Dimensional t-J Model, Phys. Rev. Lett. **88**, 117001 (2002).
[20] E. Berg, E. Fradkin, E.-A. Kim, S. A. Kivelson, V. Oganesyan, J. Tranquada, and S. Zhang, Dynamical Layer Decoupling in a Stripe-Ordered High-T_c Superconductor, Phys. Rev. Lett. **99**, 127003 (2007).
[21] Z. Xu, C. Stock, S. Chi, A. I. Kolesnikov, G. Xu, G. Gu, and J. M. Tranquada, Neutron-Scattering Evidence for a Periodically Modulated Superconducting Phase in the Underdoped Cuprate $La_{1.905}Ba_{0.095}CuO_4$, Phys. Rev. Lett. **113**, 177002 (2014).

[22] H. Jacobsen, I. A. Zaliznyak, A. T. Savici, B. L. Winn, S. Chang, M. Hücker, G. D. Gu, and J. M. Tranquada, Neutron scattering study of spin ordering and stripe pinning in superconducting $La_{1.93}Sr_{0.07}CuO_4$, Phys. Rev. B **92**, 174525 (2015).

[23] P. A. Lee, Amperean Pairing and the Pseudogap Phase of Cuprate Superconductors, Phys. Rev. X **4**, 031017 (2014).

[24] F. Yu, M. Hirschberger, T. Loew, G. Li, B. J. Lawson, T. Asaba, J. B. Kemper, T. Liang, J. Porras, G. S. Boebinger, J. Singleton, B. Keimer, L. Li, and N. P. Ong, Diamagnetic response in underdoped $YBa_2Cu_3O_{6.6}$ in high magnetic fields, arXiv:1402.7371.

[25] Z. Guguchia, A. Maisuradze, G. Ghambashidze, R. Khasanov, A. Shengelaya, and H. Keller, Tuning the static spin-stripe phase and superconductivity in $La_{2-x}Ba_xCuO_4$ ($x = 1/8$) by hydrostatic pressure, New J. Phys. **15**, 093005 (2013).

[26] R. Khasanov, Z. Guguchia, A. Maisuradze, D. Andreica, M. Elender, A. Raselli, Z. Shermadini, T. Goko, F. Knecht, E. Morenzoni, and A. Amato, High pressure research using muons at the Paul Scherrer Institute, High Pressure Res. **36**, 140 (2016).

[27] G. Gaétan, W. Wang, J. P. Attfield, A. D. Huxley, and K. V. Kamenev, Turnbuckle diamond anvil cell for high-pressure measurements in a superconducting quantum interference device magnetometer, Rev. Sci. Instrum. **81**, 073905 (2010).

[28] A. Maisuradze, B. Graneli, Z. Guguchia, A. Shengelaya, E. Pomjakushina, K. Conder, and H. Keller, Effect of pressure on the Cu and Pr magnetism in $Nd_{1-x}Pr_xBa_2Cu_3O_{7-\delta}$ investigated by muon spin rotation, Phys. Rev. B **87**, 054401 (2013).

[29] D. Andreica, Magnetic Phase Diagram in Some Kondo-Lattice Compounds: Microscopic and Macroscopic Studies, PhD, thesis, ETH-Zürich, 2001.

[30] B. Nachumi, Y. Fudamoto, A. Keren, K. M. Kojima, M. Larkin, G. M. Luke, J. Merrin, O. Tchernyshyov, Y. J. Uemura, N. Ichikawa, M. Goto, H. Takagi, S. Uchida, M. K. Crawford, E. M. McCarron, D. E. MacLaughlin, and R. H. Heffner, Muon spin relaxation study of the stripe phase order in $La_{1.6-x}Nd_{0.4}Sr_xCuO_4$ and related 214 cuprates, Phys. Rev. B **58**, 8760 (1998).

[31] A. Suter and B. M. Wojek, Musrfit: A free platform-independent framework for μSR data analysis, Physics Procedia **30**, 69 (2012).

[32] Z. Guguchia, R. Khasanov, M. Bendele, E. Pomjakushina, K. Conder, A. Shengelaya, and H. Keller, Negative Oxygen Isotope Effect on the Static Spin Stripe Order in Superconducting $La_{2-x}Ba_xCuO_4$ ($x = 1/8$) Observed by Muon-Spin Rotation, Phys. Rev. Lett. **113**, 057002 (2014).

[33] D. Shoenberg, *Superconductivity* (Cambridge University Press, Cambridge, 1954), p. 164.

[34] A. Maisuradze, A. Shengelaya, A. Amato, E. Pomjakushina, and H. Keller, Muon spin rotation investigation of the pressure effect on the magnetic penetration depth in $YBa_2Cu_3O_x$, Phys. Rev. B **84**, 184523 (2011).

[35] David F. Mross and T. Senthil, Spin- and Pair-Density-Wave Glasses, Phys. Rev. X **5**, 031008 (2015).

[36] V. J. Emery and S. A. Kivelson, Frustrated electronic phase separation and high-temperature superconductors, Physica C **209**, 597 (1993).

[37] K. M. Kojima, S. Uchida, Y. Fudamoto, I. M. Gat, M. I. Larkin, Y. J. Uemura, and G. M. Luke, Physica B **326**, 316 (2003).

[38] Y. J. Uemura, G. M. Luke, B. J. Sternlieb, J. H. Brewer, J. F. Carolan, W. N. Hardy, R. Kadono, J. R. Kempton, R. F. Kiefl, S. R. Kreitzman, P. Mulhern, T. M. Riseman, D. Ll. Williams, B. X. Yang, S. Uchida, H. Takagi, J. Gopalakrishnan, A. W. Sleight, M. A. Subramanian, C. L. Chien, M. Z. Cieplak, Gang Xiao, V. Y. Lee, B. W. Statt, C. E. Stronach, W. J. Kossler, and X. H. Yu, Universal Correlations between T_c and n_s/m^* (Carrier Density over Effective Mass) in High-T_c Cuprate Superconductors, Phys. Rev. Lett. **62**, 2317 (1989).

[39] R. Khasanov, J. Karpinski, and H. Keller, Pressure effect on the in-plane magnetic penetration depth in $YBa_2Cu_4O_8$, J. Phys.: Condens. Matter **17**, 2453 (2005).

[40] A. Shengelaya and K. A. Müller, The intrinsic heterogeneity of superconductivity in the cuprates, Europhys. Lett. **109**, 27001 (2015).

[41] R. Khasanov, A. Shengelaya, K. Conder, E. Morenzoni, I. M. Savić, and H. Keller, The oxygen-isotope effect on the in-plane penetration depth in underdoped $Y_{1-x}Pr_xBa_2Cu_3O_{7-\delta}$ as revealed by muon-spin rotation, J. Phys.: Condens. Matter **15**, L17 (2003).

[42] E. Demler, S. Sachdev, and Y. Zhang, Spin-Ordering Quantum Transitions of Superconductors in a Magnetic Field, Phys. Rev. Lett. **87**, 067202 (2001).

[43] M. Hücker, M. v. Zimmermann, M. Debessai, J. S. Schilling, J. M. Tranquada, and G. D. Gu, Spontaneous Symmetry Breaking by Charge Stripes in the High Pressure Phase of Superconducting $La_{1.875}Ba_{0.125}CuO_4$, Phys. Rev. Lett. **104**, 057004 (2010).

[44] E. S. Bozin, R. Zhong, K. R. Knox, G. Gu, J. P. Hill, J. M. Tranquada, and S. J. L. Billinge, Reconciliation of local and long range tilt correlations in underdoped $La_{2-x}Ba_xCuO_4$, Phys. Rev. B **91**, 054521 (2015).

[45] Z. Guguchia, D. Sheptyakov, E. Pomjakushina, K. Conder, R. Khasanov, A. Shengelaya, A. Simon, A. Bussmann-Holder, and H. Keller, Oxygen isotope effects on lattice properties of $La_{2-x}Ba_xCuO_4$ (x=1/8), Phys. Rev. B **92**, 024508 (2015).